RNA:DNA hybrids from Okazaki fragment contribute to establish the Ku-mediated barrier to replication fork degradation

Charlotte Audoynaud, Kamila Schirmeisen, Anissia Ait Saada, Armelle Gesnik, Paloma Fernández-Varela, Virginie Boucherit, Virginie Ropars, Anusha Chaudhuri, Karine Fréon, Jean-Baptiste Charbonnier, et al.

HAL Id: hal-04071177

https://hal.science/hal-04071177

Submitted on 17 Apr 2023

RNA:DNA hybrids from Okazaki fragment contribute to establish the Ku-mediated barrier to replication fork degradation

Charlotte Audoynaud[1,2]*, Kamila Schirmeisen[1,2]*, Anissia Ait Saada[1,2]#, Armelle Gesnik[3]#, Paloma Fernández Varela[3]#, Virginie Boucherit[1,2], Virginie Ropars[3], Anusha Chaudhuri[1,2], Karine Fréon[1,2] Jean Baptiste Charbonnier[3], Sarah AE Lambert[1,2,4]**

1. Institut Curie, Université PSL, CNRS UMR3348, 91400 Orsay, France
2. Université Paris-Saclay, CNRS UMR3348, 91400 Orsay, Ligue Nationale Contre le cancer (équipe labélisée) France
3. Université Paris-Saclay, CEA, CNRS, Institute for Integrative Biology of the Cell (I2BC), 91198, Gif-sur-Yvette, France.

* Equal contribution.

# Equal contribution.

4 Lead contact: Sarah Lambert

** Corresponding author: sarah.lambert@curie.fr

Abstract

Non-homologous end-joining (NHEJ) factors act in replication fork protection, restart and repair. Here, we identified a mechanism related to RNA:DNA hybrids to establish the NHEJ factor Ku-mediated barrier to nascent strand degradation, in fission yeast. RNase H activities promote nascent strand degradation and replication restart, with a prominent role of RNase H2 in processing RNA:DNA hybrids to overcome the Ku-barrier to nascent strand degradation. RNase H2 co-operates with the MRN-Ctp1 axis to sustain cell resistance to replication stress, in a Ku-dependent manner. Mechanistically, the need of RNaseH2 in nascent strand degradation requires the primase activity that allows establishing the Ku-barrier to Exo1 whereas impairing Okazaki fragment maturation reinforces the Ku-barrier. Finally, replication stress induces Ku foci in a primase-dependent manner and favors Ku binding to RNA:DNA hybrids. We propose a function for the RNA:DNA hybrid originating from Okazaki fragment in controlling the Ku-barrier specifying nuclease requirement to engage fork resection.

Introduction

A myriad of unavoidable replication fork obstacles threaten faithful DNA duplication [1]. As fork obstacles lead to stalling, collapse or fork breakage, they are direct sources of replication stress-induced genome instability, an underlying cause of human diseases and a well-recognized hallmark of most cancer cells [2]. Therefore, investigating the molecular circuits preserving genome integrity and replication competence at stressed replication fork is substantial to understand the etiology of human diseases.

Elongating transcription machineries are one type of fork obstacle causing fork arrest. Head-on collision upon transcription-replication conflict (TRC) triggers unscheduled R-loop formation, *i.e.* a triple-stranded structure composed of a co-transcriptionally formed RNA:DNA hybrid opposite to a displaced single-stranded DNA (ssDNA) [3,4]. Head-on TRC activates ATR-dependent DNA damage-response (DDR) pathway and R-loops formed at TRCs are detrimental to genome stability maintenance [5], although it remains unclear how the RNA:DNA hybrid itself and/or the stalled RNA polymerase contribute to fork stalling [6]. Nonetheless, several studies have established that a subset of R-loop is genotoxic [7,8].

RNA:DNA hybrids are also a consequence of double-strand break (DSB) repair [9,10]. Whereas the ways they originate at DSBs are still under debate, they are proposed to act as mediators of DSB repair and signaling [11,12]. RNA:DNA hybrids modulate the activity of DNA repair machineries allowing the recruitment of DNA repair factors from the homologous recombination (HR) and non-homologous end-joining (NHEJ) pathways [13–19]. RNA:DNA hybrids have been also proposed to mediate RNA-templated DNA repair and to influence the fidelity of DSB repair by NHEJ [20,21]. However, it is also evident that RNA:DNA hybrids at DSBs are removed or degraded to allow the completion of DNA repair, requiring therefore the activity of RNA helicases such as Senataxin or RNase H activities [10,13,16,18,22,23].

Protection, restart and repair of stressed replication fork is critical to genomic stability, giving rise to the identification of a diversity of fork rescue pathways, underscoring the plasticity of the replication fork [24]. Error-free repair of replication-born DNA damage usually relies on the HR pathway to protect nascent strand from hyper-degradation and to resume DNA replication [25]. Recent works support that NHEJ is active during DNA replication to repair stressed fork and to safeguard fork integrity [15]. In both yeast and mammals, several NHEJ-related factors, such as Ku, XLF, RIF1 and 53BP1, are engaged at stalled or broken fork to act as anti-resection barriers, independently of their canonical function in NHEJ [26–33]. Moreover, Ku binding at reversed or broken fork precedes HR activity, ensuring coordinated nascent strand degradation or Rad51 loading [27,34]. However, erroneous NHEJ event at halted fork triggers chromosomal rearrangement and therefore NHEJ-mediated fork processing is tightly regulated by mechanisms that remain poorly understood [35,36].

Many RNA species are physiologically associated to DNA replication [21]. Ribonucleotides are frequently incorporated by replicative DNA polymerases generating thousands of DNA-embedded RNA species that are further removed by RNase H2 [37,38]. During Okazaki fragment (OF) synthesis on the lagging strand, the primase synthetizes a RNA primer of 8-12 ribonucleotides in size, that is successively elongated by Pol α and δ [38,39]. OF is therefore a potential source of RNA:DNA hybrids inherently associated to the DNA replication process. Whether such physiological RNA:DNA hybrids could be modulator of replication fork repair, as proposed for DSB repair, is currently unknown. In addition, RNAs are well-described *cis* and *trans*-modulators of NHEJ activity (reviewed in [15]) but the role of RNA-associated DNA replication in regulating NHEJ function at replication stress sites has not been explored yet.

Here, we address the function of RNA:DNA hybrids during fork repair by taking advantage of a transcription-independent replication fork barrier (RFB) [40]. We employed the previously described *RTS1*-RFB that allows the polar block of a single replisome by a DNA-bound protein complex. Forks arrested at the *RTS1*-RFB are restarted in 15-20 minutes by an HR-dependent but DSB-independent mechanism, called Recombination-Dependent Replication (RDR) [41–43]. Nascent strand degradation by nucleases allows ssDNA gap to form and to recruit HR factors to promote replication restart [44]. The restarted fork is associated to a non-canonical DNA synthesis insensitive to the RFB [45–47]. We found that unprocessed RNA:DNA hybrids at the RFB prevent the degradation of nascent strand and replication restart. Nascent strand degradation relies on the catalytic activity of RNase H2 to overcome the NHEJ factor Ku-mediated barrier. We propose that the unprocessed primer of the last synthetized OF is embedded in the reversed fork, triggering an RNA:DNA hybrid formation on which Ku can bind, revealing that the RNA:DNA hybrid from OF plays a regulatory function in safeguarding fork integrity.

Results

Unresolved RNA:DNA hybrids at arrested fork impair nascent strand degradation.

RNA:DNA hybrids were shown to accumulate both upstream and downstream of the *RTS1*-RFB during S-phase [47]. To investigate the dynamics of those RNA:DNA hybrids, we performed real-time microscopy. We asked how frequently the catalytic-dead form of RNase H1 fused to GFP (Rnh1-D129N-GFP), used to detect RNA:DNA hybrids [48], co-localizes with the *LacO*-marked RFB which nuclear positioning is visualized by mCherry-LacI foci (Figure S1A). Even though *LacO*-arrays led to a background a co-localization events regardless of the activity of the RFB, RNA:DNA hybrids significantly accumulated in S-phase cells upon activation of the RFB (in 48% of cells in RFB ON versus 30% in RFB OFF, p<0.005) compared to control conditions (Figure S1B-C). Most of the co-localization events lasted for less than 40s, suggesting a short-life time and fast processing of RNA:DNA hybrids (Figure S1D). We thus questioned the origin of those RFB-induced RNA:DNA hybrids and their potential influence on fork repair.

As reported [10,49], the lack of RNase H1 and H2 activities resulted in cell sensitivity to replication blocking agents and accumulation of RNA:DNA hybrids (Figure 1A and S2A-B). Thus, we investigated the role of RNase H1 and H2 in promoting replication resumption at the RFB. The absence of RNase H1 and H2 led to a ~2-fold reduction in the frequency of replication slippage occurring downstream the RFB, a mutational signature left by HR-mediated restarted forks [45,46], indicating a reduced RDR efficiency (Figure 1B-C). By analyzing the replication intermediates (RIs) by bi-dimensional gel electrophoresis (2DGE), the formation of large ssDNA gaps (>100 bp) at the RFB resulted into a specific "tail" DNA structure, emanating from arrested fork signal and descending toward the linear arc (red arrow on Figure 1D and S2C) [27,50]. The absence of RNase H1 and H2 led to the disappearance of the "tail" signal (Figure 1D-E and S2D-E). The profile of RPA binding downstream of the RFB revealed no RPA loading in the absence of RNase H1 and H2 (Figure 1 F). This lack of ssDNA gap can be caused either by the need to process RNA:DNA hybrids to engage nascent strand degradation or by an accumulation of *de novo*, possibly transcriptionally-induced, RNA:DNA hybrids, in a post-resection manner, that would compete with RPA loading, as previously proposed [10,51,52] (Figure 1G). To distinguish between these two hypotheses, purified RIs were treated with RNase H1 *in vitro* before resolution by 2DGE. We reasoned that if ssDNA gaps are masked by *de novo* RNA:DNA hybrids *in vivo*, their processing *in vitro* should restore the "tail" signal (Figure 1 G, right panel). In contrast, if RNA:DNA hybrids need to be processed *in vivo* to engage nascent strand resection, the "tail" signal should not be restored (Figure 1G, left panel). Most RNA:DNA hybrids co-eluted with the ssDNA-enriched fraction and were fully eliminated upon RNase H1 treatment (Figure 1H), without affecting the intensity of the "tail" signal in *wild type* (*WT*) and *rnh1Δ rnh201Δ* cells (Figure 1D-E), supporting the hypothesis that unprocessed RNA:DNA hybrids at arrested fork impair nascent strand degradation *in vivo*.

The short-range resection of nascent strand requires RNA:DNA hybrids processing by RNaseH2.

We then analyzed each single RNase H mutant and found that fork-resection was 2-times decreased in *rnh201Δ* cells compared to *WT*, whereas no defect was observed in *rnh1Δ* or in the catalytic dead mutant *rnh1-D129N* cells (Figure 2A-B). The profile of RPA binding downstream of the RFB revealed that RPA loading was severely compromised only in *rnh201Δ* cells (Figure 2C), further supporting that, among the two RNase H activities, RNase H2 is mainly responsible for the degradation of nascent strand while RNase H1 may act as a backup activity. Furthermore, RNase H2 was also involved in the hyper-resection of arrested fork observed in the absence of Rad3[ATR] (Figure 2D-E) [44]. RNase H2 is involved in the processing of RNA:DNA hybrids and promotes ribonucleotide excision repair (RER) [53]. The Rnh201-G72S, an analogous Aicardi-Goutières patient mutation, is a nearly catalytic-dead form of RNase H2 [54–56], that maintains sufficient activity to prevent global RNA:DNA hybrids accumulation and resistance to replication stress when combined with *rnh1* deletion (Figure S2A-B) but was defective enough to exhibit defect in nascent strand degradation at the RFB (Figure 2A-B). In contrast, the Rnh201-RED mutant that is specifically defective for the excision of mono and di-ribonucleotides [56] showed neither accumulation of RNA:DNA hybrids nor defective nascent strand degradation (Figure 2A-B and S2B). Of note, *rnh201-RED* conferred a slight sensitivity to hydroxyurea when combined with *rnh1* deletion (Figure S2A), consistent with a higher incorporation of ribonucleotides during replication under dNTP pool starvation and cell survival relying on RER pathway [57,58]. We concluded that the ability of RNase H2 to process RNA:DNA hybrids promotes physiological and pathological nascent strand degradation.

RNase H2 counteracts the Ku-mediated barrier to nascent strand degradation by Exo1.

In fission yeast and human cells, the degradation of nascent strand is a two-step process with a short-range resection mediated by the MRN (Mre11-Rad50-Nbs1)-Ctp1 axis generating ~ 110 bp sized gaps that are obligatory for subsequent Exo1-mediated long-range resection up to ~ 1KB [27,59,60]. The profile of RPA binding downstream of the RFB indicated that RNase H2 was required for both short and long range resection, similarly to the MRN-Ctp1 axis (Figure 2C). We therefore investigated the interplays between RNase H2 and the MRN-Ctp1 axis. We found that the defects in fork-resection and in the frequency of RFB-induced replication slippage in *rad50Δ rnh201Δ* cells were similar to the ones observed in *rad50Δ* cells, indicating that RNaseH2 co-operates with MRN to promote nascent strand degradation and replication restart (Figure S3A-C). Moreover, genetic analysis revealed that defect in both RNase H2 and Rad50, or Ctp1, led to synthetic lethality upon treatment with replication-blocking agents (Figure 3A and S3D). This synthetic lethality was dependent on the catalytic activity of RNase H2 but partly alleviated when RNase H2 retains its ability to process RNA:DNA hybrids (Figure 3B). We and others, have shown that Ku restricts Exo1 activity at replication fork and that MRN-Ctp1 overcomes the Ku-mediated barrier to engage the long-range resection [27,60]. Interestingly, the synthetic lethality observed between MRN-Ctp1 axis and RNase H2 in response to replication stress was fully dependent on Ku (Figure 3Aand S3D), revealing that the ability of RNase H2 to process RNA:DNA hybrids co-operates with the MRN-Ctp1

axis to overcome Ku function during replication stress. To gauge this function, we asked if RNase H2 counteracts the Ku-mediated barrier to nascent strand degradation. The analysis of the "tail" signal revealed that in the absence of Ku, nascent strand degradation is independent of RNase H2 while remaining Exo1 dependent (Figure 3C-D), similarly to MRN-Ctp1 axis defect [27], indicating that RNase H2 processes an RNA:DNA hybrid that contributes to establish the Ku-mediated barrier to Exo1 resection. Surprisingly, we observed that the deletion of *pku70* did not rescue the fork-resection defect observed in the absence of both RNase H activities, in contrast to the rescue phenotype observed in the single *rnh201* null mutant (Figure 3C-D). These data suggest that distinct RNA:DNA hybrids form at the RFB and are processed differently by RNase H1 and H2, the latter having a specific function in regulating Ku function at arrested forks.

The nuclease activity of MRN is dispensable to overcome the Ku-mediated barrier to nascent strand degradation at the RFB [27], raising the possibility that RNase H2 may compensate for this. Nonetheless, no synthetic lethality was observed when combining *rnh201* deletion with a nuclease dead allele of *mre11* (*mre11-D65N*) neither a more drastic defect in nascent strand degradation at the RFB (Figure S3B-C). Furthermore, the MRN-Ctp1 axis was proposed to release Ku from replication-born DNA damage [27,60]. Consistent with this, Pku80-GFP foci accumulated in *rad50Δ* cells upon 4 hours of CPT treatment but such accumulation did not occur in *rnh201Δ* cells and was not exacerbated in the double mutant (Figure S4A-B) [61]. Since topoisomerase I inhibition by CPT can result in single ended DSB, we analyzed Pku80-GFP localization to the *LacO*-marked RFB and obtained similar data (Figure S4C-D). Although these data may reflect a role for MRN, in addition to promote Ku eviction from stressed fork, in limiting Ku accumulation, this function is not shared by RNase H2. We suggest that RNase H2 and MRN-Ctp1 co-operate to overcome the Ku-mediated barrier to Exo1 by providing distinct activity: RNaseH2 processes an RNA:DNA hybrid at arrested fork to offer an entry point for Exo1 activity, while limiting or evicting Ku relies on MRN-Ctp1.

Lack of RNase H activities does not impair fork reversal at the RFB

In human cells, reversed fork is an entry point for nuclease activities to promote nascent strand degradation [24,59,62] and provides a double-stranded DNA end for Ku binding as recently shown by Moldovan's lab [60]. An unresolved RNA:DNA hybrid at arrested fork may prevent fork reversal and thus nascent strand degradation. To explore this, we investigated the formation of reversed fork at the RFB. We exploited that, following restriction digestion, reversed fork would release a linear DNA fragment specific to the regressed arm, whose length corresponds to the distance between the site of fork arrest and the first restriction site upstream the RFB (Figure 4A) [63]. First, we employed a construct and a restriction digest for which the expected size of the reversed arm is of 1.1 Kb in a *rad50Δ exo1Δ* background to avoid its degradation. After RIs enrichment and resolution by 1DGE, we detected signals corresponding to the monomer (M), the arrested fork (AF) and a linear fragment of ~1.1 Kb (RA) (Figure 4B, left panel). This last signal was restricted to the RFB ON condition and detected exclusively when using a probe specific to the reversed arm (compare red

and black probes), consistent with fork reversal occurring at the active RFB. Similar results were obtained with a construct for which the expected size of the reversed arm is of 3 Kb. Consistent with this linear fragment corresponding to the reversed arm, it migrated as a smear in *WT* cells in which nascent strand degradation occurs (Figure 4B, right panel). Reversed fork is an X-shaped DNA structure detectable by 2DGE as a diagonal spike emanating from arrested fork signal [63]. Such conical signal has been reported at the fork pausing site *MPS1* in *S. pombe* and upon global replication stress in *Physarum polycephalum* [64,65]. To date, such signal was undetectable in our 2DGE blots when using a restriction enzyme cutting 1.1 Kb away from the RFB even when fork-resection is abolished in *rad50Δ exo1Δ* cells (Figure 4C, bottom panel). One explanation is that the reversed arm is cut by the restriction enzyme, leading to the loss of the X-shaped structure. To test this, we performed 2DGE using a restriction enzyme cutting 3 Kb upstream the RFB and observed an X-shaped structure emanating from fork arrest signal in *rad50Δ exo1Δ* cells but not in *WT* cells (Figure 4C, top panels). These data indicate that the detection of reversed fork by 2DGE is sensitive to the position of the restriction site relative to the fork arrest site and requires a reversed arm not being resected, consistent with fork reversal undergoing nascent strand degradation.

Breakage of the arrested fork would similarly results in the detection of the observed linear fragment. To exclude this possibility, we analyzed the dynamics of the linear fragment during cell cycle. Because of difficulties in getting well-synchronized population in a *rad50Δ exo1Δ* cells, we shifted to the single *exo1Δ* mutant in which the reversed arm, while moderately resected, was detectable by 1DGE (Figure 4D). The reversed arm appeared and disappeared concomitantly to the AF signal during S-phase progression and was not persistent in G2 cells, indicating similar kinetics resolution (Figure 4E-F). While the repair of a broken arm would rely on the HR pathway, the intensity of the linear fragment in *rad51Δ* or *rad52Δ* cells was not significantly different from *WT* cells (Figure S5B-C). We also excluded the hypothesis that the linear fragment resulted from Mus81-dependent fork cleavage (Figure S5) [66,67]. Although we cannot formally rule out that the linear fragment signal results in part from fork breakage, our data converge on most of this signal exhibiting the hallmarks of a reversed arm, consistent with arrested fork undergoing fork reversal at the RFB. Of note, despite that initial studies reported that checkpoint kinases prevent fork reversal in response HU treatment in yeast, reversed fork was observed in checkpoint proficient yeast cells upon CPT treatment [68–70]. However, we found no variation in the intensity of the reversed arm in the absence of Rad3$^{Mec1/ATR}$ (Figure S5D-E).

The lack of RNase H2 or both RNase H activities did not impact the intensity of the reversed arm (Figure 4G) revealing that fork reversal was not impaired by an unresolved RNA:DNA hybrid at the RFB and placing RNase H2 function downstream fork remodeling to overcome the Ku-mediated barrier to nascent strand degradation.

The RNA primer from Okazaki fragment is an RNase H2 substrate at arrested fork

To address the origin of the RNA:DNA hybrid at arrested fork making RNase H2 necessary to engage nascent strand degradation, we focused on Okazaki fragment (OF) metabolism as recurrent synthesis of RNA primer on the lagging strand is a source of RNA:DNA hybrids coupled to DNA replication [38]. We made use of two temperature sensitive alleles of *spp1* that encodes the primase catalytic subunit: *spp1-4* (D275G, L429P) and *spp1-21* (D74E, V180G) (Figure 5A). These mutations are consistent with a global destabilization of the Spp1 protein in a temperature-dependent manner, leading to unstable Polα-primase complex even at 25°C, affecting the synthesis of RNA primers [71]. Compared to *WT*, both primase mutants led to an hyper-resection of nascent strand that was no longer dependent on RNase H2, at both 25°C and 32°C (Figure 5B-C and S5A-B). This rescue phenotype cannot be explained by a cell growth defect or cell cycle distribution that were similar between the strains at 25°C and 32°C (Figure 5A and S6C). Hence, compromising RNA primer synthesis of OF bypasses RNase H2 requirement, supporting that OF synthesis generates an RNA:DNA hybrid processed by RNase H2 to engage Exo1 resection. Moreover, the RNA primer from OF appears critical to limit nascent strand degradation, raising the possibility that the Ku-mediated barrier to Exo1 is not fully established when the RNA primer synthesis is compromised. In support of this, CPT-induced Pku80-GFP foci were reduced by nearly 2 times in *spp1-4* and *spp1-21* cells, compared to *WT* (Figure 5D-E). We concluded that the RNA primer from OF synthesis generates an RNA:DNA hybrid that contributes to establish the Ku-mediated barrier, making RNase H2 necessary to engage nascent strand degradation.

To strengthen this conclusion, we reasoned that increasing the half-life of OF by mutating the prominent OF maturation factor Rad2^{Fen1} should reinforce the Ku-mediated barrier and dampen nascent strand degradation in a Ku-dependent manner. Fork-resection was decreased by 2 times in *rad2Δ* cells and this phenotype was rescued by deleting *pku70* (Figure 5B-C). In contrast, a defect in Sen1, an RNA helicase involved in R-loop processing [22,23,72] did not affect nascent strand degradation (Figure 5 B-C), supporting that the RNA primer from OF, but unlikely R-loop, generates an RNA:DNA hybrid to play a pivotal role in regulating nascent strand degradation by modulating the Ku-mediated barrier.

Ku binds to OF *in vitro* and to RNA:DNA hybrids *in vivo* upon replication stress

Collectively, our data led us to hypothesize that the reversed arm embeds the last unligated OF being annealed to its complementary nascent leading strand, making RNase H2 necessary to process the resulting RNA:DNA hybrid to offer an entry point to Exo1 activity, thus counteracting Ku-mediated barrier to nascent strand degradation. This model implies that Ku binds to RNA:DNA hybrids. In CPT (4 hours, 20μM) treated cells, immuno-precipitated Pku70-HA associated with RNA:DNA hybrids, as revealed with the S9.6 antibody. No S9.6 signal was enriched in control strains and untreated condition (Figure 6A). Such Ku-RNA:DNA hybrids interaction did not result from an higher expression of Pku70-HA upon CPT treatment (Figure 6B). To gauge if RNA:DNA hybrids are direct substrates of Ku, we investigated the interaction of purified *S. pombe* Ku (SpKu) with

RNA:DNA hybrid by biophysical methods. We co-expressed *S. pombe* Pku70 and Pku80 in insect cells and purified the complex at homogeneity in large quantity for calorimetry analyses (Figure S7A). We first measured the affinity of SpKu for double-strand DNA (dsDNA), the classical DNA substrate of Ku in canonical NHEJ and measured a Kd of 0.9 ± 0.04 nM (Figure 6C-E, substrate A, and S7 for sequences). This represents a slightly higher affinity compared to the affinity measured by calorimetry with human Ku and the same DNA substrate [73]. We then designed two substrates with one biotin at an extremity or two biotins at both extremities to block them with streptavidin (Substrates B and C, respectively on Figure 6D). We observed an interaction with one extremity blocked in the nanomolar range though with a weaker affinity (Kd of 41 ± 3 nM) and no interaction with the DNA blocked at the two ends (Figure 6C and 6E, substrates B and C). We then designed a DNA with the same sequence except that one strand contains 10 ribonucleotides in 5' followed by 8 deoxyribonucleotides. This molecule mimics an OF substrate. We blocked one end by using a biotin and streptavidin (Figure 6D, substrate D compared to B). We measured an interaction with a tight affinity, Kd of 5.8 ± 2.9 nM (Figure 6C and 6E, substrate D). We then designed a substrate with an hairpin as an alternative way to block one extremity. We observed also a tight interaction in the nanomolar range (Kd of 10 ± 0.2 nM) (Figure 6C and 6E, substrate E). These two last measurements indicate that SpKu interacts tightly *in vitro* with OF substrates. Finally, we designed a substrate that mimics an OF not present at an extremity but in an internal position as in a lagging strand (Figure 6D, substrate F). We observed no interaction of SpKu with this molecule suggesting that Ku interaction with OF requires the RNA:DNA hybrid to be accessible from an extremity (Figure 6E, substrate F). We cross-validated these calorimetry results with EMSA analyses that show a similar interaction between dsDNA and a substrate containing an OF (Figure S7B-DC). Overall, we concluded that RNA:DNA hybrids are physiological substrates for Ku binding in response to replication stress and that Ku is able to bind substrates mimicking OF *in vitro.*

Discussion

Collectively, this study uncovers an RNA:DNA hybrid-related mechanism to regulate the Ku-mediated barrier to nascent strand degradation. We propose that the RNA primer originating from OF synthesis is embedded in the reversed arm of reversed fork, creating a substrate for Ku binding and specifying nuclease requirement to engage fork resection (Figure 7). The coordinated action of MRN-Ctp1 axis and RNase H2 promotes Ku eviction and the RNA:DNA hybrid degradation, respectively, allowing Exo1 to degrade nascent strand. This RNA:DNA hybrid-based mechanism contributes to safeguard fork integrity and timely replication resumption, revealing an underappreciated function for DNA-embedded RNA species in maintaining genome stability.

Several individual NHEJ-related factors are involved in fork protection, in repairing replication-induced DSBs and in restarting replication fork [15]. In fission yeast, Ku binding to arrested fork is necessary for recovery from replication stress by promoting timely fork restart and fork protection [27,47]. Human RIF1, 53BP1 and KU have been proposed to act as barriers against nascent strand degradation and thus to contribute to fork protection and prevent under-replicating DNA leading to chromosome breakage [26–29]. Recently, the Moldovan's lab demonstrated that human KU association to HU-stalled fork depends on fork reversal at which the KU-PARP14 axis is part of a multistep process to regulate nascent strand degradation [60]. In contrast, the Smolka's lab showed that KU-DNAPK stabilizes HU-stalled fork by promoting fork reversal and subsequent nascent strand degradation [74]. While these reports underscore the importance of regulating NHEJ-mediated fork protection pathways, they also suggest that human KU may act at multiple steps during fork-protection. Since there is no DNAPK orthologue identified so far in yeast, we favor the hypothesis that *S. pombe* Ku is recruited at arrested fork downstream fork reversal but this remains to be formally demonstrated.

RNAs are known *cis* and *trans*-modulators of NHEJ activity, in particular during DSB repair [15]. Here, we propose that RNA:DNA hybrids are *cis*-regulators of Ku function at reversed fork to regulate nascent strand degradation. Beyond the *RTS1*-RFB scenario, we establish that Ku binds RNA:DNA hybrid upon replication stress and substrates mimicking OF. Moreover, defects in RNase H2 and MRN lead to synthetic lethality upon replication stress, in a Ku-dependent manner. The synthesis of OF on the lagging strand is a recurrent source of RNA:DNA hybrids associated to DNA replication. Compromising the RNA primer synthesis of OF bypasses RNase H2 requirement and impairs the Ku-mediated barrier to nascent strand degradation. In human cells, two pathways of replication fork protection were identified providing distinct nuclease substrates and engagement of distinct fork protection factors [28]. We speculate that the presence of the last unprocessed OF, embedded as an RNA:DNA hybrid within the reversed arm of the reversed fork, may provide substrate specificity for nucleases and Ku binding. In this scenario, overcoming the Ku-barrier would require nucleases able to process the RNA:DNA hybrid from OF such as RNase H2 whereas the absence of RNA:DNA hybrids may generate a reversed arm with an extremity not suitable for Ku binding

(Figure 7). Of note, RIF1 and 53BP1 promote fork-protection by counteracting DNA2-dependent resection, a nuclease previously involved in OF processing [26,28,29].

At DSBs, short and long-range resection are coordinated by a complex interplay between Ku and MRN-CtIP[Ctp1], with Ku being an early responder to restrict the long-range resection [75]. In both fission yeast and mammalian cells, Ku eviction from DSB ends depends on MRN-CtIP[Ctp1] and Mre11 nuclease activity [34,76]. Recently, Ku protein block was proposed to stimulate Mre11-mediated initial endonucleolytic cleavage of 5'-terminated DNA strands, promoting a switch toward short-range resection [60,77]. In yeasts, MRN promotes nascent strand degradation at the *RTS1*-RFB and stalled forks, in a nuclease-independent manner [27,78]. The presence of an RNA:DNA hybrid within the reversed arm constitutes an additional level of complexity in the understanding of MRN and Ku antagonism in controlling fork-resection. One hypothesis is that MRN-Ctp1 is inefficient in promoting 5' incision at an RNA:DNA hybrid, as previously suggested [79], requiring additional nuclease activities to promote long-range resection. However, we obtained no evidences that nascent strand degradation depends on the nuclease activity of Mre11 in primase mutant. We propose that RNase H2, by processing RNA:DNA hybrids, likely provides nicks used as an entry point for Exo1 activity, therefore overcoming the Ku-mediated barrier [80]. In such a scenario, Ku eviction remains dependent on MRN-Ctp1 but independent of Mre11 nuclease activity, a mechanism that remains to be understood. Moreover, in the absence of RNase H2 and Ku, nascent strand degradation depends on Exo1, suggesting that Exo1 is able to process the RNA moiety of an RNA:DNA hybrid. *In vitro*, Exo1 can degrade RNA:DNA hybrids containing up to 10 consecutive ribonucleotides, but not 15 [81]. The RNA primer during OF synthesis ranges from 8 to 12 ribonucleotides [38] raising the possibility that Exo1 can process them at a low rate, explaining the partial fork-resection defect in the absence of RNase H2, unless additional nucleases are acting at an RNA:DNA hybrid-containing reversed fork (Figure 7).

Mutations in any of the 3 subunits of RNase H2 account for more than half of the Aicardi-Goutières syndrome (AGS) cases, an autoimmune genetic disorder characterized by an upregulation of type I interferon (IFN) expression and microcephaly [54]. To date, the molecular tenants of this pathology are still unclear. Another gene frequently mutated in AGS is SAMHD1 that has been recently involved in nascent strand degradation at HU-stalled forks in human cells [82]. Mechanistically, SAMHD1 stimulates the exonuclease activity of MRE11 to allow replication restart. In SAMHD1-depleted cells, alternative processing of stalled forks by RECQ1 leads to ssDNA accumulation in the cytoplasm that in turn triggers cGAS-STING pathway activation and IFN production. Our work establishes that fission yeast RNase H2 also contributes to fork-resection, further linking AGS to defect in nascent strand degradation and fork restart, consistent with patient-derived AGS cells carrying defect in RNase H2 exhibit signs of replication stress and chronic activation of the DDR, in particular of the post-replication repair pathway [83].

The role of DNA-embedded RNAs species in regulating fork repair has received little attention so far. We propose that RNA:DNA hybrids embedded in reversed fork and originating from OF are *cis-regulators* of Ku function to maintain replication fork integrity. We uncover a role for RNA:DNA hybrids in dictating requirement for specific dismantling activities to ensure proper replication fork processing and restart.

Limitation of the study

We propose reversed fork as an entry point for Ku binding and nuclease activities, as suggested in humans. So far, we are unable to delineate the genetic requirement for fork reversal in yeast, likely because multiple helicases or translocases are involved as found in human, preventing us to test further the model. However, we do not exclude that fork-resection can occur independently of fork reversal. Moreover, our data establish that the primase activity is critical to control the Ku-mediated barrier to nascent strand degradation and our results indicate a role of OF in this process. Nonetheless, we cannot exclude that the primase may also fill-in the resected reversed arm via the fission yeast ST complex, analogue to the human CST complex. Finally, consistent with the defect of fork resection in the absence of RNase H activities being not rescued by the deletion of Ku, we do not exclude that additional replication stress-induced RNA:DNA hybrids may be at work at replication stress sites to regulate DNA repair pathway and maintain genome integrity.

Acknowledgements

Author contributions

CA performed the experiments on Figure 1, 2, 3, 5B-C (*rad2Δ* and *sen1Δ*), 6 A-B, S1, S2, S3D-F, S4. AAS and VB performed the experiments of Figure 4 and S5. PFV, AG and VR performed the experiments on Figure 6 C-D and S7. KS performed the experiments on Figure 5A-C, S3A-C and S6. AC performed the experiments on figure 5D-E. KF contributed to all experiments, excepted 6C-D and S7, via her contribution to lab management and direct involvement in performing experiments. CA, KF, KS, JBC and SAEL contributed to experimental design and data analysis and presentation. CA, JBC and SAEL wrote the manuscript. JBC and SAEL edited the manuscript.

Declaration of interest

The authors declare no competing interests.

Figure 1

A

	Untreated	HU 3mM	CPT 5µM	MMS 0.005%	Bleocin 0.025µM
WT					
rnh1Δ					
rnh201Δ					
rnh202Δ					
rnh203Δ					
rnh1Δ rnh201Δ					
rnh1Δ rnh202Δ					
rnh1Δ rnh203Δ					
rad52Δ					

B

Main replication direction

RFB
ura4-sd20
ori
Cen 3

Fork arrest
HR-mediated restart

C

Frequency of RFB-induced RS (X 10⁻³)

ns   ns   ns   0.0004   <0.0001   <0.0001

WT   rnh1Δ   rnh201Δ   rnh1Δ rnh201Δ   rnh1Δ rnh202Δ   rnh1Δ rnh203Δ

D

RFB ON

Arrested fork
Secondary signal
Resected fork

	untreated	+ RNase H
WT	97.6±1.9	98.2±1.4
rnh1Δ rnh201Δ	99±0.6	98.1±0.7

F

RPA enrichment (RFB ON/RFB OFF ratio)

WT
rnh1Δ rnh201Δ

0.003   <0.0001   <0.0001   0.003   0.001   0.004

-110   110   400   600   900   1400

RFB   ori

G

Pre-resection   Post-resection

↓RNase H

Tail signal -   Tail signal +

E

WT   rnh1Δ rnh201Δ

% of resected forks (relative to arrested forks)

<0.0001

ns

ns

RNase H   -   +   -   +

H

dsDNA   S9.6   ssDNA   S9.6

WT
rnh1Δ rnh201Δ
WT
rnh1Δ rnh201Δ
WT
rnh1Δ rnh201Δ

DNaseI RNaseH1

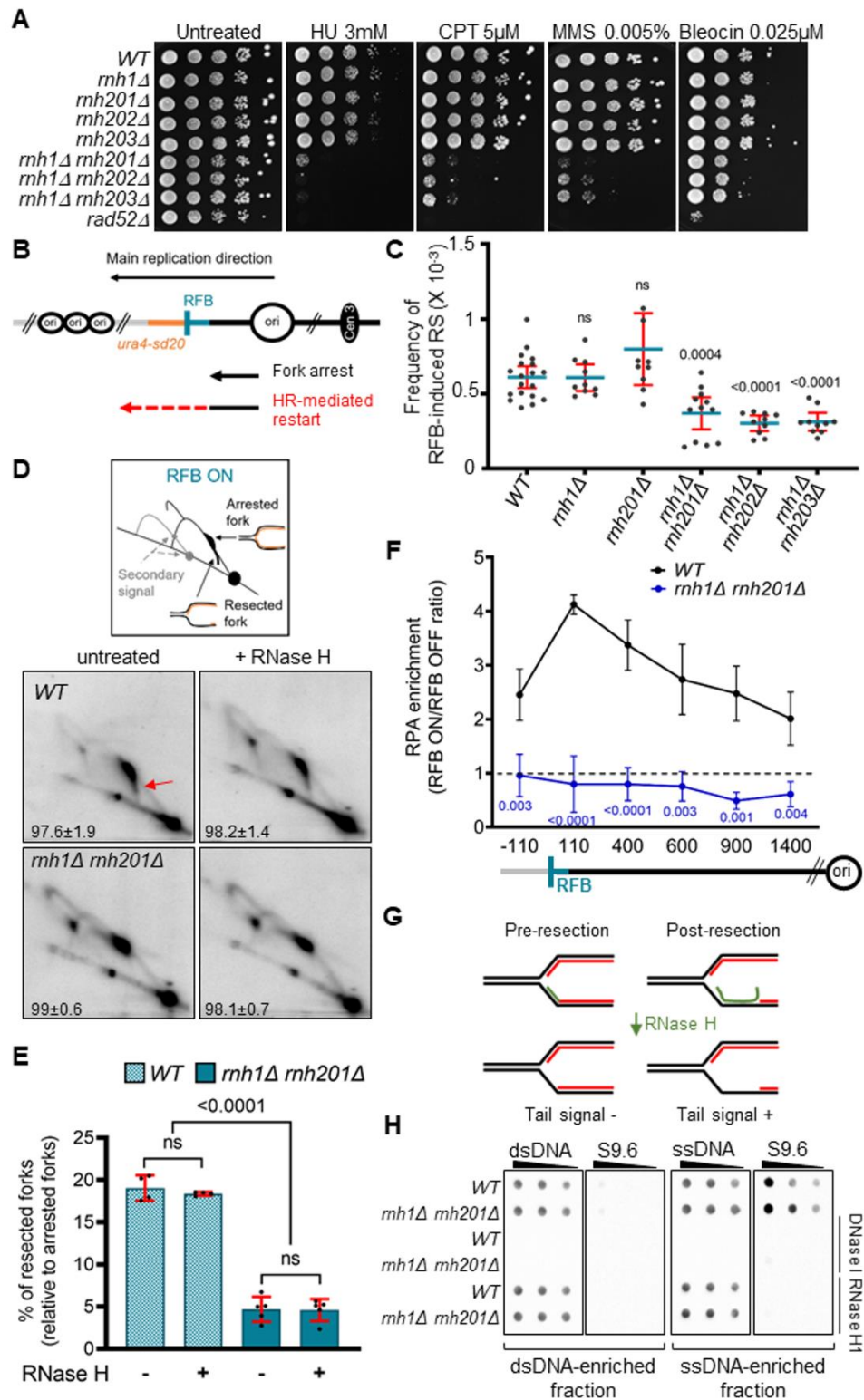dsDNA-enriched fraction   ssDNA-enriched fraction

14

Figure 1: RNaseH activities promote nascent strand degradation and recombination-dependent replication.

(A) Tenfold serial dilutions of indicated strains on indicated media conditions (CPT: camptothecin, HU: hydroxyurea, MMS: methyl methane sulfonate).

(B) Diagram of the *t-ura4sd20<ori* construct containing a single *RTS1*-RFB (<, blue bars) that leads to the polar arrest of replisomes traveling from the centromere (Cen3) toward the telomere (t). "Ori" (black circles) indicate the main replication origins upstream and downstream the RFB. Polar fork arrest is mediated by the binding of Rtf1 to the *RTS1* sequence. Rtf1 expression in under the thiamine-repressible *nmt41* promoter: with thiamine, Rtf1 is repressed and the RFB is poorly active (RFB OFF); without thiamine, Rtf1 is expressed and the RFB is strongly active (RFB ON) (REF). The non-functional *ura4-sd20* allele contains a 20 nt duplication flanked by micro-homology. HR-mediated restart is associated to a non-canonical DNA synthesis prone to frequent replication slippage (RS) leading to the deletion of the duplication, thus restoring a functional *ura4+* marker [45].

(C) Frequency of RFB-induced RS in indicated strains and conditions. Each dot represents one sample from independent biological replicate. Bars indicate mean values ± 95 % confidence interval. Statistics were calculated using Mann-Whitney U test, compare to *WT*.

(D) RIs analysis by neutral-neutral 2DGE. Top: Scheme of RIs observed within the *AseI* restriction fragment in RFB ON condition using *ura4* as probe. Gray lines indicate secondary signal caused by partial digestion of psoralen-cross linked RIs. Bottom: representative 2DGE analysis in indicated strains in RFB ON condition, with RIs treated or not with RNase H *in vitro*. The red arrow indicates the "tail" signal in *WT* strain. Numbers indicate the efficiency of the RFB ± standard deviation (SD).

(E) "Tail" quantification from panel C. Dots represent values obtained from independent biological replicates. Bars indicate mean values ± SD. Statistical analysis was performed using student's t-test.

(F) Analysis of RPA recruitment (ON/OFF ratio) to the *RTS1*-RFB by ChIP-qPCR in indicated strains. Distances from the RFB are indicated in base pairs (bp). Values are means of at least three independent experiments ± SD. Statistical analysis was performed using student's t-test, compared to *WT*.

(G) Scheme of hypothetic models explaining how an RNA:DNA hybrid may interfere with ssDNA gaps in a pre or post-resection manner. The green lines indicate an RNA:DNA hybrid.

(H) Separation of digested and psoralen-cross linked DNA samples on BND-cellulose columns resulted in a dsDNA and a ssDNA-enriched fractions which were treated *in vitro* with RNase H1 or DNase I and analyzed by dot blot using anti-dsDNA (dsDNA), anti-ssDNA (ssDNA) and S9.6 antibodies.
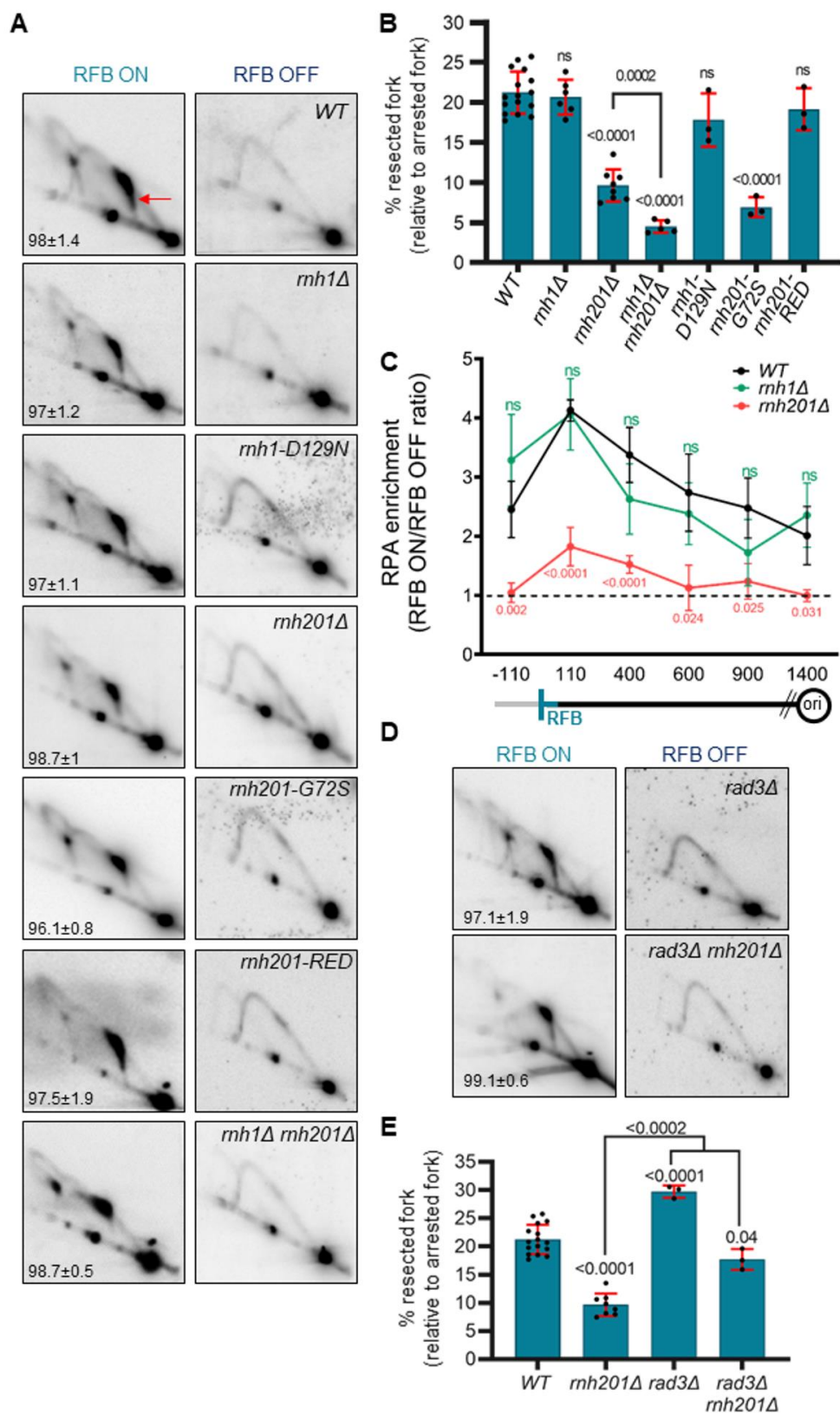
See also Figure S1, S2,Table S1 and S2.

Figure 2

Figure 2: RNase H2-mediated processing of RNA:DNA hybrids engages nascent strand degradation.

(A) and (D) Representative 2DGE analysis in indicated strains and conditions as described in 1D.

(B) and (E) "Tail" quantification from panel C. Dots represent values obtained from independent biological replicates. Bars indicate mean values ± SD. Statistical analysis was performed using student's t-test.

(C) Analysis of RPA recruitment (ON/OFF ratio) to the *RTS1*-RFB by ChIP-qPCR in indicated strains. Distances from the RFB are indicated in base pairs (bp). Values are means of at least three independent experiments ± SD. Statistical analysis was performed using student's t-test, compared to *WT*.

See also Figure S2, Table S1 and S2.

Figure 3
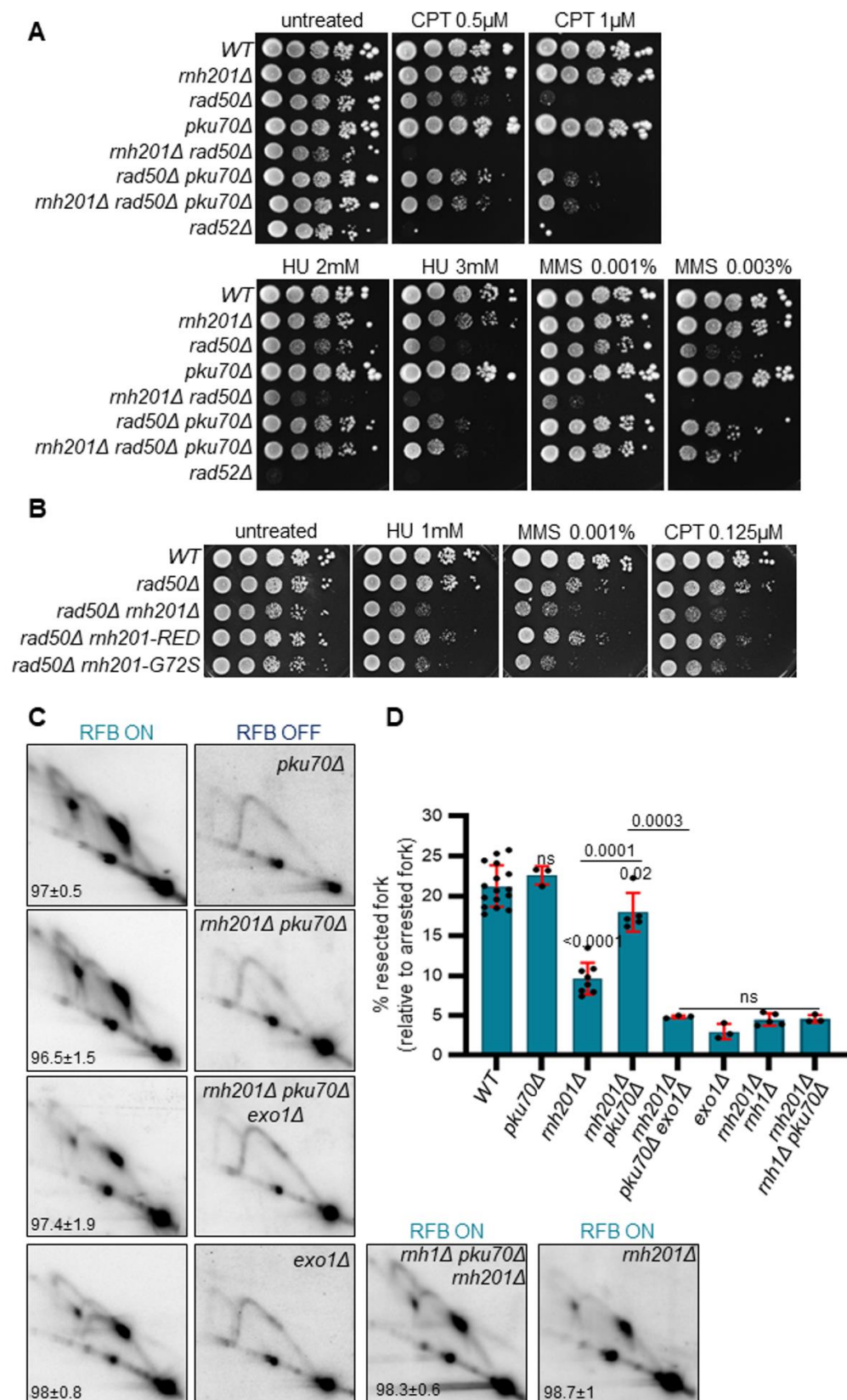
Figure 3: RNase H2 co-operates with MRN to overcome Ku-mediated barrier to resection.

(A) and (B) Tenfold serial dilutions of indicated strains on indicated media conditions (CPT: camptothecin, HU: hydroxyurea, MMS: methyl methane sulfonate).

(C) Representative 2DGE analysis in indicated strains and conditions as described in 1D.

(D) "Tail" quantification from panel C. Dots represent values obtained from independent biological replicates. Bars indicate mean values ± SD. Statistical analysis was performed using student's t-test.

See also Figure S3, S4 and Table S1.

Figure 4

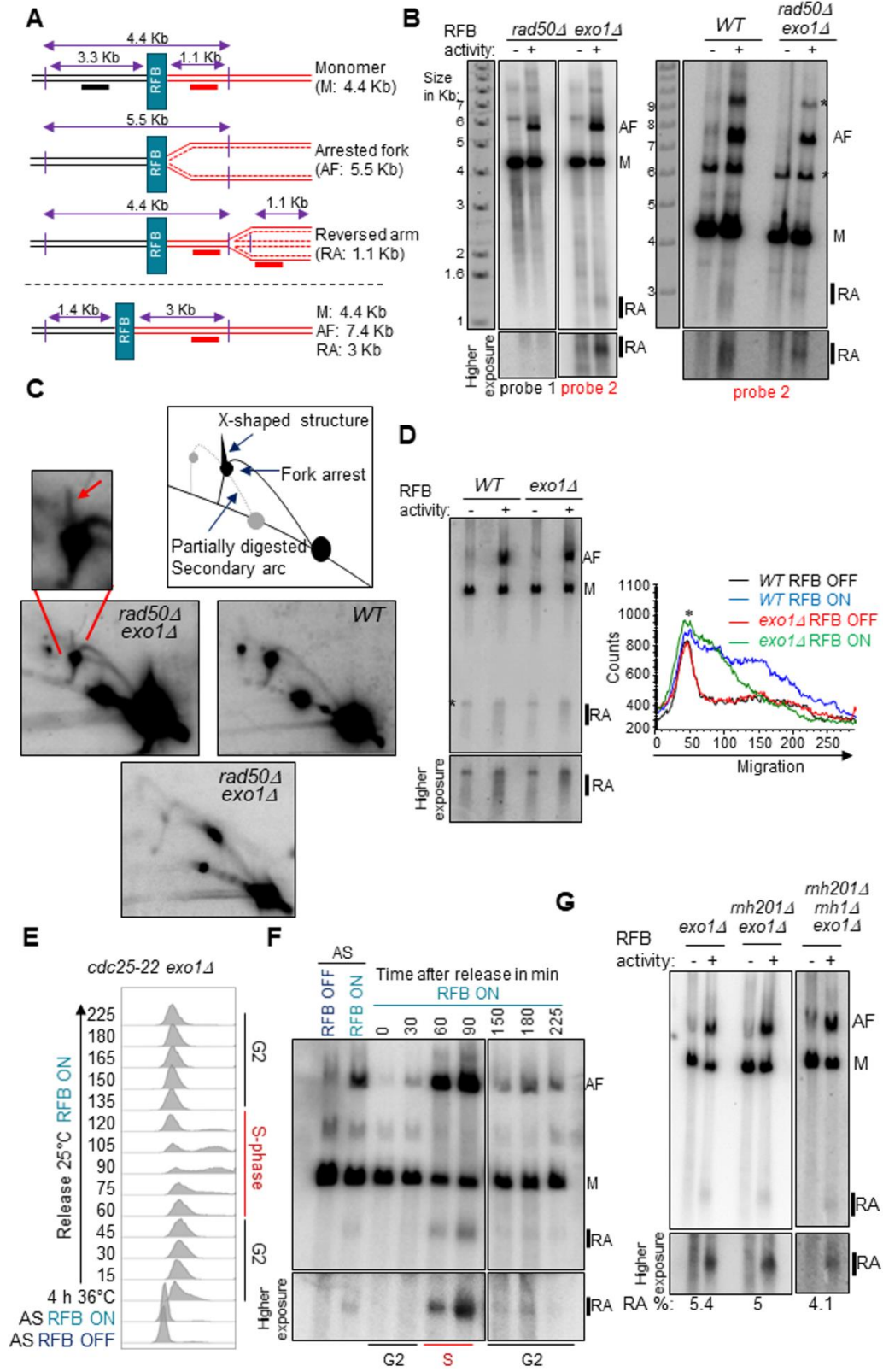**Figure 4: Fork reversal at the RFB is not impaired by unresolved RNA:DNA hybrids**

(A) Scheme of the constructs used with the expected mass of RIs species and the probes used (Probe 1 and 2 in black and red, respectively).

(B) Representative Southern-blot analysis after 1DGE resolution of RIs in indicated strains and conditions, using indicated probes. A higher exposure of the RA is shown. * indicates partial digestion caused by psoralen-crosslinks. 1.1 Kb-RA and 3 Kb-RA constructs, as described in panel A, on left and right, respectively.

(C) Top panel: Scheme of RIs observed within the *AseI* restriction fragment in RFB ON condition using the probe 2 (red) and the 3Kb-RA construct described in panel A. Gray lines indicate secondary signal caused by partial digestion of psoralen-cross linked RIs. Middle panel: representative 2DGE analysis in indicated strains in RFB ON condition. The red arrow indicates signal corresponding to fork reversal. Bottom panel: 2DGE analysis in RFB ON condition using the probe 2 (red) and the 1Kb-RA construct described in panel A.

(D) Left panel: Representative Southern-blot analysis after 1DGE resolution of RIs in indicated strains and conditions, using the probe 2 (red) and the 1.1 Kb-RA construct described in panel A. Right panel: corresponding scan lines of RA intensity according to migration distance for each strain and condition. The unspecific band marked by * was used as reference.

(E) Flow cytometry analysis of *cdc25-22 exo1Δ* cells synchronized in G2 (4hours at 36°C) and released in cell cycle at 25°C in RFB ON condition. Time points are indicated in minutes. AS: asynchronous cells.

(F) Southern-blot analysis after 1DGE resolution of RIs from cell synchronization described in panel E, using the probe 2 (red) and the 3 Kb-RA construct described in panel A.

(G) Representative Southern-blot analysis after 1DGE resolution of RIs in indicated strains and conditions using the probe 2 (red) and the 1.1 Kb-RA construct described in panel A. Number indicate the estimation of % RA relative to arrested fork (AF) signal.

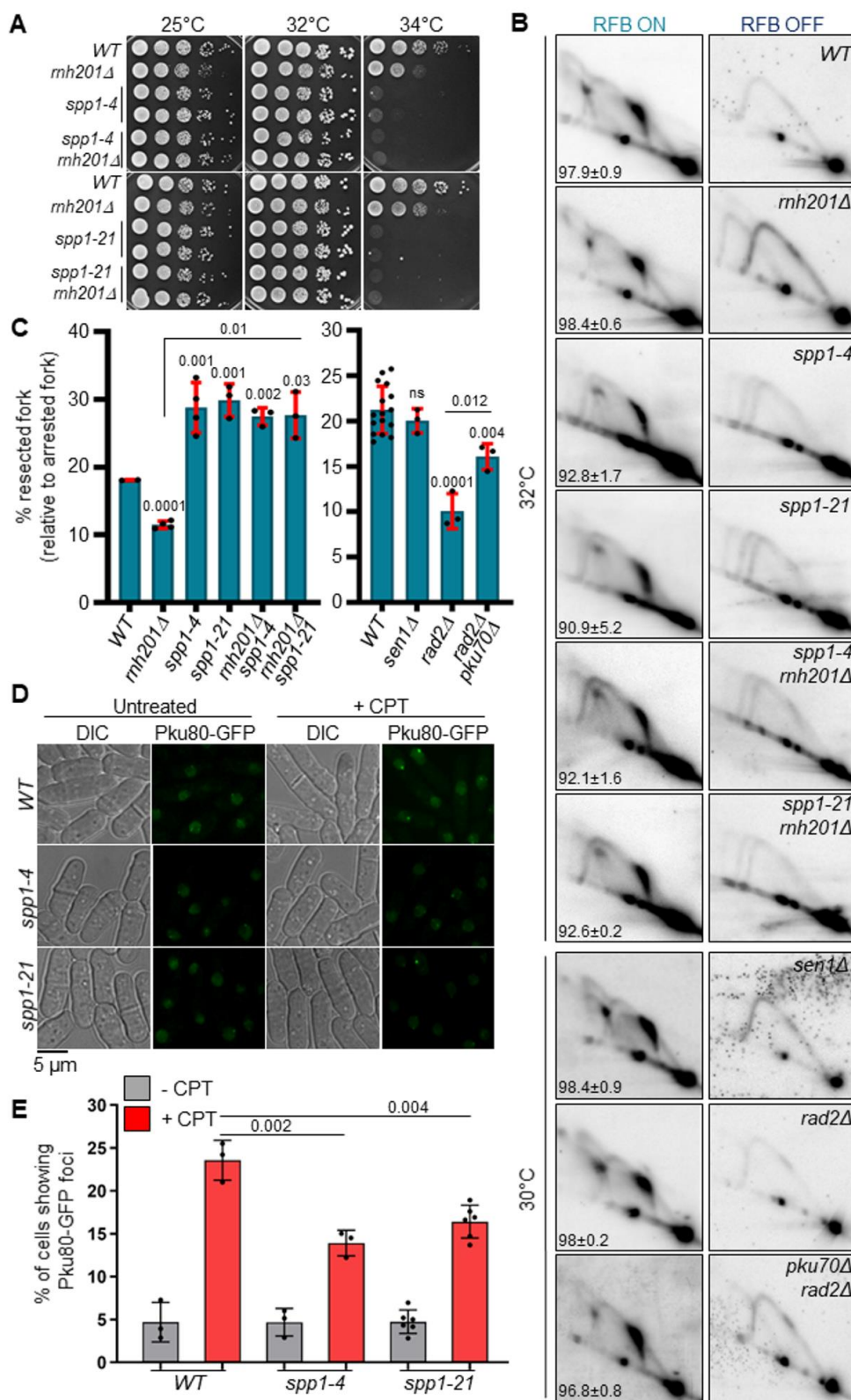See also Figure S5 and Table S1.

Figure 5

Figure 5: Interfering with Okazaki fragment synthesis and maturation affects the requirement for RNase H2 activity and the Ku-mediated barrier.

(A) Tenfold serial dilutions of indicated strains at indicated temperatures.

(B) Representative 2DGE analysis in indicated strains and conditions as described in 1D. The 32°C panels correspond to strains that were grown at 25°C and shifted at 32°C for 19 hours.

(C) "Tail" quantification from panel B. Dots represent values obtained from independent biological replicates. Bars indicate mean values ± SD. Statistical analysis was performed using student's t-test.

(D) Examples of cells showing Pku80-GFP foci in indicated strains and conditions (CPT at 20µM for 4 hours). Strains were grown at 25°C and shifted to 32°C for 19 hours before CPT treatment.

(E) Quantification of panel D. Dots represent values obtained from independent biological replicates. Bars indicate mean values ± SD. At least 500 nuclei were analyzed for each experiment. Statistical analysis was performed using student's t-test.

See also Figure S6 and Table S1.

Figure 6
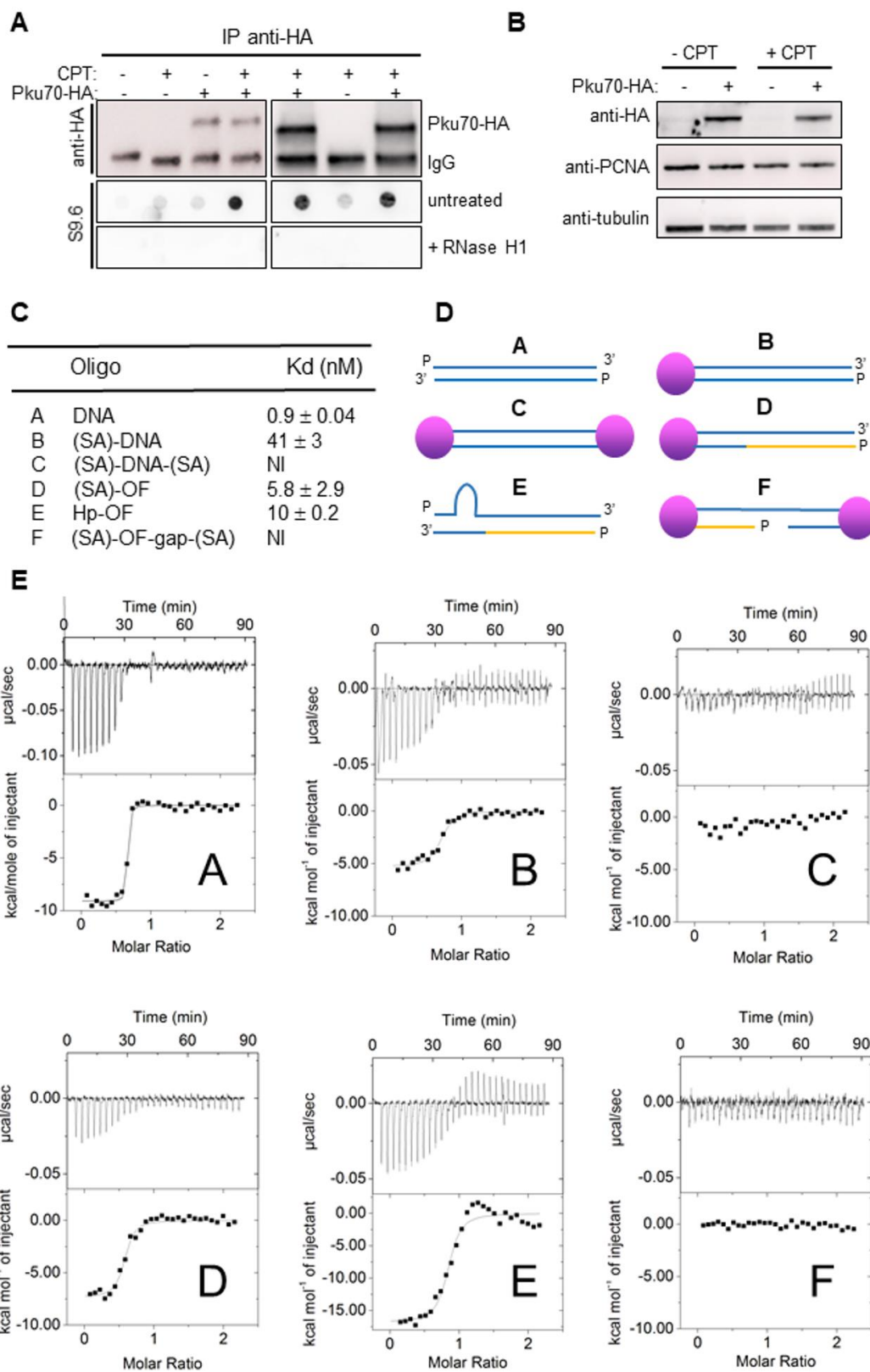
Figure 6: Ku binds RNA:DNA hybrids related substrates *in vivo* and *in vitro*.

(A) Analysis of RNA:DNA hybrids co-immnuno-precipitated with anti-HA antibody in indicated strains and conditions. Top panel: Immunoblots using anti-HA antibody. The position of Pku70-HA and IgG are indicated. Bottom panels: detection of RNA:DNA hybrids by dot blot using S9.6 antibody. Treatment with RNaseH1 *in vitro* revealed the specificity of the signal.

(B) Expression of Pku70-HA by immuno-blot in indicated strains and conditions. Tubulin and PCNA were used as loading control.

(C-D) Calorimetry measurements of the interaction between SpKu and several substrates: dsDNA 18bp, without (A) or with one (B) or two streptavidin (C) blocking the extremities. Substrate (D) equivalent to (B) with an OF fragment at one end. Substrate (E) with an OF fragment and an hairpin as a blocking function. Substrate (F) with an OF fragment in the internal position and 4 nucleotides gaps (see Figure S7 for sequences of the substrates).

(E) Thermograms and Isothermal Titration Curves of SpKu with the substrates A to F.

See also Figure S7, Table S1 and S2.

Figure 7

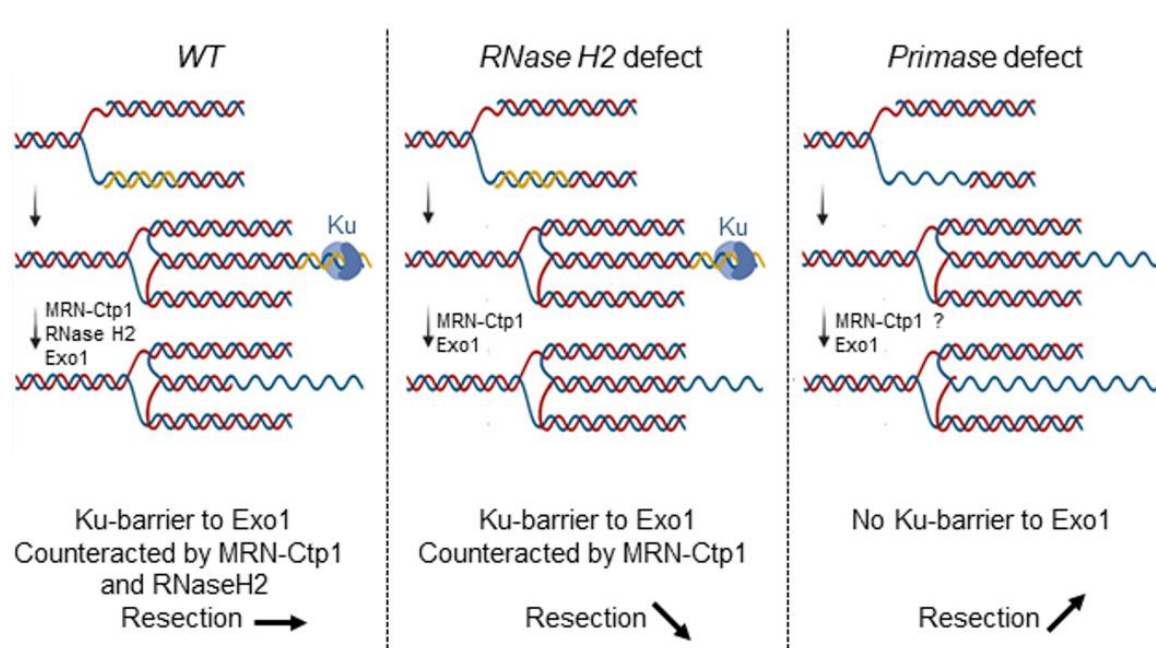Figure 7: The RNA primer from Okazaki fragment contributes to establish the Ku-mediated barrier and thus specifying nuclease requirement (see text for details).

RESOURCE AVAILABILITY

Lead contact

Further information and requests for reagents and resources should be directed to and will be fulfilled by the Lead Contact, Dr. Sarah A.E. Lambert (sarah.lambert@curie.fr)

Materials Availability

All unique/stable reagents generated in this study are available from the lead contact without restriction.

Data and Code availability

● Data have been deposited to Mendeley data and are publicly available as the date of publication. DOIs are listed in the key resources table (https://data.mendeley.com/datasets/k5xm5fpyxt).

● This paper does not report original code.

● Any additional information required to reanalyze the data reported in this paper is available from the lead contact upon request.

EXPERIMENTAL MODEL AND SUBJECT DETAILS

Yeast strains were freshly thawed from frozen stocks and grown at 25 °C or 30 °C using standard yeast genetics practices.

MATERIEL AND METHODS

Standard yeast genetics

Yeast strains used in this study are listed in Supplementary Table S1. The *rnh201-G72S* mutant was obtained by classical genetic techniques. Strains carrying the *RTS1*-RFB system were grown in supplemented EMM-glutamate, where the *RTS1*-RFB barrier was kept inactive by adding 60 µM thiamine (condition RFB OFF). To induce fork blockade, cells were washed twice in water and cultivated in fresh thiamine-free medium for 24 hours incubation (condition RFB ON). For *spp1-4* temperature-sensitive mutants, cells were grown at the permissive temperature of 25 °C in the RFB OFF condition, and then shifted to the semi-permissive temperature of 32 °C for 19 hours prior RFB induction. To assess the sensitivity of chosen mutants to genotoxic drugs, exponentially growing cultures were serially diluted and spotted onto plates containing hydroxyurea (HU), campthotecin (CPT) or methyl methanesulfonate (MMS).

Replication slippage assay

5-FOA (EUROMEDEX, 1555) resistant colonies were grown on uracil-containing plates with or without thiamine for 2 days at 30 °C. They were subsequently inoculated into EMMg supplemented with uracil, with or without thiamine, for 24 hours. Cells were diluted and plated on EMMg complete (for cell survival) and on EMMg uracil-free plates, both supplemented with 60 µM thiamine. To determine the reversion frequency, colonies were counted after 5 to 7 days of incubation at 30 °C as previously described [45].

Analysis of replication intermediates by 2DGE

Exponentially growing cells (2.5×10^9) were treated with 0.1% sodium azide and mixed with frozen EDTA. Genomic DNA was crosslinked upon trimethyl psoralen (0.01 mg/mL, TMP, Sigma, T6137) addition to cell suspensions, for 5 min in the dark with occasional swirling. Then, cells were irradiated with UV-A (365 nm) for 90 s at a constant flow of 50 mW/cm^2 [84]. Cell lysis was performed using 0.625 mg/mL lysing enzymes (Sigma, L1412) and 0.5 mg/mL zymolyase 100 T (Amsbio, 120493-1). Resulting spheroplasts were embedded into 2 % low-melting agarose (Lonza, 50081) plugs. Next, plugs were incubated overnight at 55 °C, in a digestion buffer with 1 mg/mL of proteinase K (Euromedex, EU0090), prior washing and storage in TE buffer (50 mM Tris, 10 mM EDTA) at 4 °C. DNA digestion was performed using 60 units per plug of restriction enzyme *Ase*I (NEB, R0526M). Samples were treated with beta-agarase (NEB, M0392L) and RNase A (Roche, 11119915001) and equilibrated to 0.3 M NaCl. Replication intermediates (RIs) were purified using BND cellulose columns (Sigma, B6385; Biorad, 731-1550), as previously described [41]. Double-stranded DNA (dsDNA) was eluted by washing with 0.8 M NaCl, 10mM Tris-HCl (pH 7.5), and 1 mM EDTA. DNA containing single-stranded regions (ssDNA), such as RIs, was eluted by addition of 3 ml of 1 M NaCl, 10 mM Tris-HCl (pH 7.5), 1 mM EDTA, and 1.8% caffeine (Sigma, C-8960). RIs were precipitated with glycogen (Roche, 1090139001) and then separated by two-dimensional electrophoresis using 0.35 % and 0.9 % (+EtBr) agarose gels (1xTBE) for the first and second dimensions, respectively. Migrated DNA was transferred to a nylon membrane (Perkin-Elmer, NEF988001PK) in 10x SSC and probed with ^{32}P-radiolabeled *ura4* probe (TaKaRa *Bca*BEST™ Labeling Kit, 6046 and alpha-^{32}P dCTP, Perkin-Elmer, BLU013Z250UC) in Ultra-Hyb buffer (Invitrogen, AM8669) at 42°C. Signal of replication intermediates was collected in phosphor-imager software (Typhoon-trio) and quantified by densitometric analysis with ImageQuantTL software (GE healthcare). The 'tail signal' was normalized to the overall signal corresponding to arrested forks (see Figure S2A for a detailed explanation)

For the *in vitro* treatment of purified RIs with RNase H1 (NEB, M0297L), the following modifications were performed. Samples were treated with RNase T1 (Thermo Scientific, EN0541) instead of RNase A. Eluted DNA fractions enriched in dsDNA and ssDNA were both precipitated and washed with 70 % EtOH. 3 μg of isolated DNA was saved for the dotblot analysis. The rest was processed for 2DGE analysis: half was digested 2 hours at 37 °C with RNase H1 before migration on the first dimension.

Fork reversal detection by 1DGE

RIs were prepared as described above for 2DGE analysis. For *Asc*I-containing constructs (Figures 4D-G, S5), DNA digestion was done with 30 units per plug of restriction enzyme *Ava*I (NEB, R0152M). After the first dimensional migration, 0.35 % agarose gels were stained with EtBr. Crosslinks were reversed by UV-c (254nm) irradiation (5.555 kJ/m^2) before transfer to a nylon membrane. Transfer was performed using a vacuum machine in 0.5N NaOH for 1 hour and 50 min, at 50mBar. Membranes' probing was performed as for 2DGE. Probe 1 (Figure 4B, left panel) and Probe 2 used to detect the 3Kb-RA (Figure 4B, right panel) correspond to the *ura4* probe. The probes used to detect the 1Kb-RA (Figures 4 and S4) were made using *L3* primer combined either with *L600* (Figure 4B, left panel) or *Ase1Cen* (see primers list in Supplementary Table S2, Related to Key Resources Table of STAR methods section).

Nucleic acid extraction

2.5×10^8 cells from exponentially growing cultures were harvested, washed in water and resuspended in 600 µL of lysis solution (2% Triton X-100, 1% SDS, 0.1 M NaCl, 10 mM Tris pH 8, 1 mM EDTA) and 600 µL phenol-chloroform. Cell lysis was performed with a Precellys homogenizer. After lysate clarification, nucleic acids were precipitated by adding cold 100% EtOH. Resulting pellets were then washed in cold 70% EtOH, air dried and let to resuspend into 100µL of water overnight at 4 °C.

Dot blot

Before blotting, all DNA samples were evenly split and submitted to the following digestions. 4µg DNA of each sample were treated with 6U RNase III (NEB, M0245L) for 2 hours at 37°C, followed by inactivation for 20 min at 65°C. As controls, for each sample, the same amount of DNA was additionally treated with 10U RNase H1 (NEB, M0297L) or 50U DNase I (Worthington Biochemical, LS006333). All digested products were diluted to an equal concentration in 2x SSC and then serially diluted. 200µL of the resulting dilutions were spotted onto a Nylon membrane (Perkin-Elmer, NEF988001PK), using a dot blot apparatus. Spotting was performed in replicates on the same membrane, that is subsequently cut to isolate replicates that will be incubated for 2 hours 30 min with the following antibodies: S9.6 (I. Curie, 1:5.000 in TBS-Tween 5% milk), α-dsDNA (Santa Cruz, Sc-58749; 1:5.000 in TBS-Tween 5% BSA) or α-ssDNA (Millipore, MAB3034; 1:10.000 in TBS-Tween 5% BSA). Goat anti-mouse HRP conjugate (Jackson ImmunoResearch, 115-035-003) was used as secondary antibody and was incubated with all membranes (1:10.000 in TBS-Tween 5% milk) for 1 hour. Blotting and all incubations were done at room temperature.

Flow cytometry

Flow cytometry analysis of DNA content was performed as described previously [85]. Briefly, cells fixed in 70 % EtOH were washed with 50 mM sodium citrate then digested with RNase A (Sigma, R5503) for 2 hours and stained with 1µM Sytox Green nucleic acid stain (Invitrogen, S7020). Samples were subjected to flow cytometry using FACSCANTO II (BD Biosciences). For Figure S6C, asynchronous cell populations were analysed using the flow cytometric method that exploit the width and the total area of the DNA-associated signal to discriminate G1 and G2 phases [86].

Live cell imaging

All image acquisition was performed on the PICT-IBiSA Orsay Imaging facility of Institut Curie. For snapshot microscopy, in RFB OFF and RFB ON conditions, cells were grown in filtered supplemented EMM-glutamate, with or without thiamine respectively, for 24 hours. Exponentially growing cultures were centrifuged and resuspended in 50 µL of fresh medium. 2 µL from this concentrated solution was dropped onto a Thermo Scientific slide (ER-201B-CE24) covered with a thin layer of 1.4 % agarose in filtered EMMg. 13 z-stack pictures (each z step of 300 nm) were captured using a Spinning Disk Nikon inverted microscope equipped with the Perfect Focus System, Yokogawa CSUX1 confocal unit, Photometrics Evolve512 EM-CCD camera, 100X/1.45-NA PlanApo oil immersion objective and a laser bench (Errol) with 491 and 561 nm diode lasers, 100 mX (Cobolt). Pictures were collected with METAMORPH software and analyzed with ImageJ. To investigate the colocalization between Pku80-GFP and *lacO*-bound mCherry-LacI, both channels were merged. Foci that merged or partially overlap were counted as colocalization event.

For the analysis of Pku80-GFP foci formation in response to CPT treatment, cells were grown in complete media and 20µM CPT was added 4 hours prior slide preparation. Cells were visualized with a Nikon inverted microscope as described above, using only a 491 nm diode laser, 100 mX (Cobolt). Pictures were collected with METAMORPH software and analyzed with ImageJ.

Pku80-GFP foci required observer-based thresholding before analysis [61]. Threshold was put as the same level for each genetic background analyzed within the same experiment. Data were collected from at least 3 independent biological repeats.

Movie analysis

To study the colocalization time between the *LacO*-marked RFB (LacI foci) and Rnh1-D129N-GFP foci, cells were prepared and visualized with a Nikon inverted microscope as described above, using two fluorescent channels with 491 and 561 nm diode lasers, 100 mX (Cobolt). Images were captured every 10 s with 21 optical slices (each z step of 200 nm) for 45 min with 200 ms exposure time both for GFP and mCherry channels, using METAMORPH software. Movies have been mounted using ImageJ. To investigate the colocalization between Rnh1-D129N-GFP and *lacO*-bound mCherry-LacI, both channels were merged. The duration of colocalization events was estimated based on the overlap of *RTS1*-RFB *LacO*/lacI-mCherry and Rnh1-D129N-GFP signals (Figure S1).

Chromatin Immunoprecipitation (ChIP)

Chromatin immunoprecipitations against RPA (Ssb3-YFP) were performed as described in [44] with the following modifications. 2x100 mL of culture (at $1x10^7$ Cells/ml density) for each condition (*RTS1*-RFB OFF/ON) was crosslinked with 10 mM DMA (dimethyl adipimidate, thermo scientific, 20660) and subsequently 1% formaldehyde (Sigma, F-8775). Each duplicate was frozen in liquid nitrogen and then lysed by bead beating in 400 µL of lysis buffer (50 mM HEPES pH 7.5, 1 % Triton X100, 0.1 % Nadeoxycholate, 1 mM EDTA with 1 mM PMSF and Complete EDTA-free protease inhibitor cocktail tablets (Roche, 1873580). Chromatin sonication was performed using a Diagenode Bioruptor in a High mode (10 cycles of 30s ON and 30s OFF). For each condition, duplicates were pooled (2x400 µL of sonicated chromatin) and overnight immunoprecipitation was performed as follows: 300 µL was incubated with anti-GFP antibody (Invitrogen, A11122) at 1:150 while 300 µL was incubated with Normal Rabbit IgG antibody (Cell Signaling Technology, #2729S) at concentration 1:75. 5 µL was preserved as INPUT fraction. Next morning Dynabeads Protein G (Invitrogen, 10003D) were added for 1 hour and immunoprecipitated complexes have been decrosslinked for 2 hours at 65°C. DNA was purified with a Qiaquick PCR purification kit (QIAGEN, 28104) and eluted in 400 µL of water. qPCR (iQ SYBR green supermix, Biorad, 1708882, primers listed in Supplementary Table S2, Related to Key Resources Table of STAR methods section) was performed to determine the relative amounts of DNA. Calculated starting quantity values (based on standard curves for each pair of primers) were normalized by substracting the rabbit IgG control signal from the specific GFP signal. RPA enrichment is presented as ON/OFF ratio.

Pku70-3xHA ChIP was performed as described in [27]. Briefly, experiments were performed as follows: samples were crosslinked with 1 % formaldehyde for 15 min. Sonication was performed using a Diagenod Bioruptor at High setting for 8 cycles (30s ON and 30s OFF). Immunoprecipitation was performed using 50 µl anti-HA antibody coupled to magnetic beads (Thermo Scientific, Pierce 88837) for 600µl of sonicated chromatin. Cell lysis and immunoprecipitation steps were performed

in presence of RNase inhibitors (10 units/sample of RNasIN® Plus, Promega, N261B). Crosslink was reversed over night at 70°C, followed by proteinase K treatment. DNA was purified using Qiaquick PCR purification kit and eluted in 40 µl of water.

Whole protein extract analysis

Aliquots of $2x10^7$ cells from the cultures used for Pku70-3HA ChIP experiments were collected. Cells were disrupted by bead beating in 1 mL of 20 % TCA (Sigma, T9159). Pellets of denatured proteins were washed with 1M Tris pH 8 and resuspended in 2x Laemmli buffer (62.5 mM Tris pH 6.8, 20 % glycerol, 2 % SDS, 5 % β-mercaptoethanol with bromophenol blue). Samples were boiled before being subjected to SDS-PAGE on Mini-PROTEAN TGX Precast Gel 4-15 % (Biorad, 4561086). Western blot using anti-HA (Santa Cruz Biotechnology, sc-57592) or anti-tubulin (Abcam, Ab6160) antibodies was performed.

Purification of S. pombe Ku70-80

Full-length PKu70 and PKu80 were co-expressed in Sf21 insect cells and used for calorimetry and EMSA analyses. A 10His-tag was added on the N-terminus of PKu80. Protein production was initiated in Sf21 cells by infection with the baculovirus stock at MOI of 5x10-3 and cells were collected 5-6 days after the infection (3-4 days after the proliferation arrest). Cells were sonicated and the supernatant was incubated with Benzonase (300 units for 30 min at 4°C). The Ku heterodimer was purified on a NiNTA-Agarose affinity column (Protino, Macherey Nagel) with a 1M NaCl wash step to remove DNA excess. The eluted Ku was then bound onto an anion exchange column (Resource Q, GE Healthcare) equilibrate with buffer Q (20 mM Tris pH 8.0, 50 mM NaCl, 50 mM KCl, 10 mM β-mercaptoethanol). The final yield was ~4 mg of purified heterodimer by liter of culture [73].

Calorimetry

Interactions between Ku and DNA or RNA:DNA substrates were determined by isothermal titration calorimetry (ITC) using a VP-ITC calorimeter (Malvern). Prior to measurements, all solutions were degassed under vacuum. The reaction cell of the ITC (volume 1.8 mL) was loaded with Ku heterodimers. Proteins were extensively dialyzed against 20 mM Tris, pH 8.0, 150 mM NaCl, and 5 mM β-mercaptoethanol. The Ku heterodimer present in the cell was titrated by automatic injections of 10 µL of the different DNA and OF substrates. Enthalpy ΔH (in $kcal.mol^{-1}$), stoichiometry of the reaction N, and association constant Ka (in M^{-1}) were obtained by nonlinear least-squares fitting of the experimental data using the single set of independent binding sites model of the Origin software provided with the instrument. Control experiments were performed with DNA and OF molecules injected into the buffer to evaluate the heat of the dilution. The experiments were performed at 25°C. The sequences of the substrates used for the calorimetry are reported in Fig S7.

EMSA

Binding reactions (10 µL) were performed by incubating Ku and the annealed oligonucleotides listed above. One oligonucleotides is labelled with a FAM fluorophore. They are used at a final concentration of 40nM, with the indicated final concentrations of proteins in 10mM Tris-HCl pH8, 50mM NaCl (with 5% Glycerol). Reactions were incubated at 4°C for 30 minutes and fractionated by 6% PAGE (19%/1% [w/v] Acrylamide:Bis-acrylamide) in 0.5x standard Tris-borate- EDTA (TBE)

buffer at 80 V for 45 min at 4°C. After electrophoresis, DNA was visualized using a ChemiDoc MP imaging system (Bio-Rad) by direct detection of the fluorescently labeled DNA (FAM).

The sequences of the substrates used for EMSA are reported in Supplementary Table S2 (list of primers used in this study, Related to Key Resources Table of STAR methods section).

QUANTIFICATION AND STATISTICAL ANALYSIS

Quantitative densitometric analysis of Southern-blots was performed using ImageQuant software. The 'tail signal' of resected forks was normalized to the overall signal of arrested forks.

Cell images were collected using METAMORPH software. They were processed and analyzed using ImageJ software.

Definitions of represented values and error bars are mentioned within the figure legends. For most experiments, the number of samples is n > 3, obtained from independent biological replicate to ensure biological reproducibility.

Statistical analysis was carried using Mann-Whitney U tests and Student's t test, as mentioned within the figure legends.

References

1. Zeman, M.K., and Cimprich, K.A. (2014). Causes and consequences of replication stress. Nat. Cell Biol. *16*, 2–9. https://doi.org/10.1038/ncb2897.

2. Gaillard, H., García-Muse, T., and Aguilera, A. (2015). Replication stress and cancer. Nat. Rev. Cancer *15*, 276–280. https://doi.org/10.1038/nrc3916.

3. García-Muse, T., and Aguilera, A. (2019). R Loops: From Physiological to Pathological Roles. Cell *179*, 604–618. https://doi.org/10.1016/j.cell.2019.08.055.

4. Crossley, M.P., Bocek, M., and Cimprich, K.A. (2019). R-Loops as Cellular Regulators and Genomic Threats. Mol. Cell *73*, 398–411. https://doi.org/10.1016/j.molcel.2019.01.024.

5. Hamperl, S., Bocek, M.J., Saldivar, J.C., Swigut, T., and Cimprich, K.A. (2017). Transcription-Replication Conflict Orientation Modulates R-Loop Levels and Activates Distinct DNA Damage Responses. Cell *170*, 774-786.e19. https://doi.org/10.1016/j.cell.2017.07.043.

6. Kemiha, S., Poli, J., Lin, Y.L., Lengronne, A., and Pasero, P. (2021). Toxic R-loops: Cause or consequence of replication stress? DNA Repair (Amst). *107*, 103199. https://doi.org/10.1016/j.dnarep.2021.103199.

7. Promonet, A., Padioleau, I., Liu, Y., Sanz, L., Biernacka, A., Schmitz, A.L., Skrzypczak, M., Sarrazin, A., Mettling, C., Rowicka, M., et al. (2020). Topoisomerase 1 prevents replication stress at R-loop-enriched transcription termination sites. Nat. Commun. *11*, 3940. https://doi.org/10.1038/s41467-020-17858-2.

8. Costantino, L., and Koshland, D. (2018). Genome-wide Map of R-Loop-Induced Damage Reveals How a Subset of R-Loops Contributes to Genomic Instability. Mol. Cell *71*, 487-497.e3. https://doi.org/10.1016/j.molcel.2018.06.037.

9. Marnef, A., and Legube, G. (2021). R-loops as Janus-faced modulators of DNA repair. Nat. Cell Biol. *23*, 305–313. https://doi.org/10.1038/s41556-021-00663-4.

10. Ohle, C., Tesorero, R., Schermann, G., Dobrev, N., Sinning, I., and Fischer, T. (2016). Transient RNA-DNA Hybrids Are Required for Efficient Double-Strand Break Repair. Cell *167*, 1001–1013. https://doi.org/10.1016/j.cell.2016.10.001.

11. Domingo-Prim, J., Bonath, F., and Visa, N. (2020). RNA at DNA Double-Strand Breaks: The Challenge of Dealing with DNA:RNA Hybrids. BioEssays *42*, e1900225. https://doi.org/10.1002/bies.201900225.

12. Pessina, F., Giavazzi, F., Yin, Y., Gioia, U., Vitelli, V., Galbiati, A., Barozzi, S., Garre, M., Oldani, A., Flaus, A., et al. (2019). Functional transcription promoters at DNA double-strand breaks mediate RNA-driven phase separation of damage-response factors. Nat. Cell Biol. *21*, 1286–1299. https://doi.org/10.1038/s41556-019-0392-4.

13. D'Alessandro, G., Whelan, D.R., Howard, S.M., Vitelli, V., Renaudin, X., Adamowicz, M., Iannelli, F., Jones-Weinert, C.W., Lee, M.Y., Matti, V., et al. (2018). BRCA2 controls DNA:RNA hybrid level at DSBs by mediating RNase H2 recruitment. Nat. Commun. *9*, 5376. https://doi.org/10.1038/s41467-018-07799-2.

14. Michelini, F., Pitchiaya, S., Vitelli, V., Sharma, S., Gioia, U., Pessina, F., Cabrini, M., Wang, Y., Capozzo, I., Iannelli, F., et al. (2017). Damage-induced lncRNAs control the DNA damage response through interaction with DDRNAs at individual double-strand breaks. Nat. Cell Biol. *19*, 1400–1411. https://doi.org/10.1038/ncb3643.

15. Audoynaud, C., Vagner, S., and Lambert, S. (2021). Non-homologous end-joining at challenged replication forks: an RNA connection? Trends Genet. *37*, 937–985. https://doi.org/10.1016/j.tig.2021.06.010.

16. Sessa, G., Gómez-González, B., Silva, S., Pérez-Calero, C., Beaurepere, R., Barroso, S., Martineau, S., Martin, C., Ehlén, Å., Martínez, J.S., et al. (2021). BRCA2 promotes DNA-RNA hybrid resolution by

DDX5 helicase at DNA breaks to facilitate their repair. EMBO J. *40*, e106018. https://doi.org/10.15252/embj.2020106018.

17. Dang, T.T., and Morales, J.C. (2020). Xrn2 links RNA: Dna hybrid resolution to double strand break repair pathway choice. Cancers (Basel). *12*, 1–15. https://doi.org/10.3390/cancers12071821.

18. Li, L., Germain, D.R., Poon, H.-Y., Hildebrandt, M.R., Monckton, E.A., McDonald, D., Hendzel, M.J., and Godbout, R. (2016). DEAD Box 1 Facilitates Removal of RNA and Homologous Recombination at DNA Double-Strand Breaks. Mol. Cell. Biol. *36*, 2794–2810. https://doi.org/10.1128/mcb.00415-16.

19. Bhatia, V., Valdés-Sánchez, L., Rodriguez-Martinez, D., and Bhattacharya, S.S. (2018). Formation of 53BP1 foci and ATM activation under oxidative stress is facilitated by RNA:DNA hybrids and loss of ATM-53BP1 expression promotes photoreceptor cell survival in mice. F1000Research *7*, 1233. https://doi.org/10.12688/F1000RESEARCH.15579.1.

20. Chakraborty, A., Tapryal, N., Venkova, T., Horikoshi, N., Pandita, R.K., Sarker, A.H., Sarkar, P.S., Pandita, T.K., and Hazra, T.K. (2016). Classical non-homologous end-joining pathway utilizes nascent RNA for error-free double-strand break repair of transcribed genes. Nat. Commun. *7*, 13049. https://doi.org/10.1038/ncomms13049.

21. Zong, D., Oberdoerffer, P., Batista, P.J., and Nussenzweig, A. (2020). RNA: a double-edged sword in genome maintenance. Nat. Rev. Genet. *21*, 651–670. https://doi.org/10.1038/s41576-020-0263-7.

22. Cohen, S., Puget, N., Lin, Y.L., Clouaire, T., Aguirrebengoa, M., Rocher, V., Pasero, P., Canitrot, Y., and Legube, G. (2018). Senataxin resolves RNA:DNA hybrids forming at DNA double-strand breaks to prevent translocations. Nat. Commun. *9*, 533. https://doi.org/10.1038/s41467-018-02894-w.

23. Rawal, C.C., Zardoni, L., Di Terlizzi, M., Galati, E., Brambati, A., Lazzaro, F., Liberi, G., and Pellicioli, A. (2020). Senataxin Ortholog Sen1 Limits DNA:RNA Hybrid Accumulation at DNA Double-Strand Breaks to Control End Resection and Repair Fidelity. Cell Rep. *31*, 107603. https://doi.org/10.1016/j.celrep.2020.107603.

24. Berti, M., Cortez, D., and Lopes, M. (2020). The plasticity of DNA replication forks in response to clinically relevant genotoxic stress. Nat. Rev. Mol. Cell Biol. *21*, 633–651. https://doi.org/10.1038/s41580-020-0257-5.

25. Ait Saada, A., Lambert, S.A.E., and Carr, A.M. (2018). Preserving replication fork integrity and competence via the homologous recombination pathway. DNA Repair (Amst). *71*, 135–147. https://doi.org/10.1016/j.dnarep.2018.08.017.

26. Mukherjee, C., Tripathi, V., Manolika, E.M., Heijink, A.M., Ricci, G., Merzouk, S., de Boer, H.R., Demmers, J., van Vugt, M.A.T.M., and Ray Chaudhuri, A. (2019). RIF1 promotes replication fork protection and efficient restart to maintain genome stability. Nat. Commun. *10*, 3287. https://doi.org/10.1038/s41467-019-11246-1.

27. Teixeira-Silva, A., Ait Saada, A., Hardy, J., Iraqui, I., Nocente, M.C., Fréon, K., and Lambert, S.A.E. (2017). The end-joining factor Ku acts in the end-resection of double strand break-free arrested replication forks. Nat. Commun. *8*, 1982. https://doi.org/10.1038/s41467-017-02144-5.

28. Liu, W., Krishnamoorthy, A., Zhao, R., and Cortez, D. (2020). Two replication fork remodeling pathways generate nuclease substrates for distinct fork protection factors. Sci. Adv. *6*, eabc3598. https://doi.org/10.1126/sciadv.abc3598.

29. Garzón, J., Ursich, S., Lopes, M., Hiraga, S. ichiro, and Donaldson, A.D. (2019). Human RIF1-Protein Phosphatase 1 Prevents Degradation and Breakage of Nascent DNA on Replication Stalling. Cell Rep. *27*, 2558–2566. https://doi.org/10.1016/j.celrep.2019.05.002.

30. Chen, B.R., Quinet, A., Byrum, A.K., Jackson, J., Berti, M., Thangavel, S., Bredemeyer, A.L., Hindi, I., Mosammaparast, N., Tyler, J.K., et al. (2019). XLF and H2AX function in series to promote replication fork stability. J. Cell Biol. *218*, 2113–2123. https://doi.org/10.1083/jcb.201808134.

31. Sánchez, A., and Russell, P. (2015). Ku Stabilizes replication forks in the absence of Brc1. PLoS One

10, e0126598. https://doi.org/10.1371/journal.pone.0126598.

32.   Miyoshi, T., Kanoh, J., and Ishikawa, F. (2009). Fission yeast Ku protein is required for recovery from DNA replication stress. Genes to Cells *14*, 1091–1103. https://doi.org/10.1111/j.1365-2443.2009.01337.x.

33.   Joshi, R.R., Ali, S.I., and Ashley, A.K. (2019). DNA Ligase IV Prevents Replication Fork Stalling and Promotes Cellular Proliferation in Triple Negative Breast Cancer. J. Nucleic Acids, 9170341. https://doi.org/10.1155/2019/9170341.

34.   Chanut, P., Britton, S., Coates, J., Jackson, S.P., and Calsou, P. (2016). Coordinated nuclease activities counteract Ku at single-ended DNA double-strand breaks. Nat. Commun. *7*, 12889. https://doi.org/10.1038/ncomms12889.

35.   Balmus, G., Pilger, D., Coates, J., Demir, M., Sczaniecka-Clift, M., Barros, A.C., Woods, M., Fu, B., Yang, F., Chen, E., et al. (2019). ATM orchestrates the DNA-damage response to counter toxic non-homologous end-joining at broken replication forks. Nat. Commun. *10*, 87. https://doi.org/10.1038/s41467-018-07729-2.

36.   Britton, S., Chanut, P., Delteil, C., Barboule, N., Frit, P., and Calsou, P. (2020). ATM antagonizes NHEJ proteins assembly and DNA-ends synapsis at single-ended DNA double strand breaks. Nucleic Acids Res. *48*, 9710–9723. https://doi.org/10.1093/nar/gkaa723.

37.   Lazzaro, F., Novarina, D., Amara, F., Watt, D.L., Stone, J.E., Costanzo, V., Burgers, P.M., Kunkel, T.A., Plevani, P., and Muzi-Falconi, M. (2012). RNase H and postreplication repair protect cells from ribonucleotides incorporated in DNA. Mol. Cell *45*, 99–110. https://doi.org/10.1016/j.molcel.2011.12.019.

38.   Burgers, P.M.J., and Kunkel, T.A. (2017). Eukaryotic DNA replication fork. Annu. Rev. Biochem. *86*, 417–438. https://doi.org/10.1146/annurev-biochem-061516-044709.

39.   Balakrishnan, L., and Bambara, R.A. (2013). Okazaki fragment metabolism. Cold Spring Harb. Perspect. Biol. *5*, a010173. https://doi.org/10.1101/cshperspect.a010173.

40.   Lambert, S., Watson, A., Sheedy, D.M., Martin, B., and Carr, A.M. (2005). Gross chromosomal rearrangements and elevated recombination at an inducible site-specific replication fork barrier. Cell *121*, 689–702. https://doi.org/10.1016/j.cell.2005.03.022.

41.   Lambert, S., Mizuno, K., Blaisonneau, J., Martineau, S., Chanet, R., Fréon, K., Murray, J.M., Carr, A.M., and Baldacci, G. (2010). Homologous recombination restarts blocked replication forks at the expense of genome rearrangements by template exchange. Mol. Cell *39*, 346–359. https://doi.org/10.1016/j.molcel.2010.07.015.

42.   Mizuno, K., Miyabe, I., Schalbetter, S.A., Carr, A.M., and Murray, J.M. (2012). Recombination-restarted replication makes inverted chromosome fusions at inverted repeats. Nature *493*, 246–249. https://doi.org/10.1038/nature11676.

43.   Nguyen, M.O., Jalan, M., Morrow, C.A., Osman, F., and Whitby, M.C. (2015). Recombination occurs within minutes of replication blockage by RTS1 producing restarted forks that are prone to collapse. Elife *4*, e04539. https://doi.org/10.7554/eLife.04539.

44.   Tsang, E., Miyabe, I., Iraqui, I., Zheng, J., Lambert, S.A.E., and Carr, A.M. (2014). The extent of error-prone replication restart by homologous recombination is controlled by Exo1 and checkpoint proteins. J. Cell Sci. *127*, 2983–2994. https://doi.org/10.1242/jcs.152678.

45.   Iraqui, I., Chekkal, Y., Jmari, N., Pietrobon, V., Fréon, K., Costes, A., and Lambert, S.A.E. (2012). Recovery of Arrested Replication Forks by Homologous Recombination Is Error-Prone. PLoS Genet. *8*, e1002976. https://doi.org/10.1371/journal.pgen.1002976.

46.   Jalan, M., Oehler, J., Morrow, C.A., Osman, F., and Whitby, M.C. (2019). Factors affecting template switch recombination associated with restarted DNA replication. Elife *8*, e41697. https://doi.org/10.7554/eLife.41697.

47.   Naiman, K., Campillo-Funollet, E., Watson, A.T., Budden, A., Miyabe, I., and Carr, A.M. (2021).

Replication dynamics of recombination-dependent replication forks. Nat. Commun. *12*, 923. https://doi.org/10.1038/s41467-021-21198-0.

48. Chédin, F., Hartono, S.R., Sanz, L.A., and Vanoosthuyse, V. (2021). Best practices for the visualization, mapping, and manipulation of R-loops. EMBO J. *40*, e106394. https://doi.org/10.15252/embj.2020106394.

49. Zhao, H., Zhu, M., Limbo, O., and Russell, P. (2018). RNase H eliminates R-loops that disrupt DNA replication but is nonessential for efficient DSB repair. EMBO Rep. *19*, e45335. https://doi.org/10.15252/embr.201745335.

50. Ait Saada, A., Teixeira-Silva, A., Iraqui, I., Costes, A., Hardy, J., Paoletti, G., Fréon, K., and Lambert, S.A.E. (2017). Unprotected Replication Forks Are Converted into Mitotic Sister Chromatid Bridges. Mol. Cell *66*, 398-410.e4. https://doi.org/10.1016/j.molcel.2017.04.002.

51. Liu, S., Hua, Y., Wang, J., Li, L., Yuan, J., Zhang, B., Wang, Z., Ji, J., and Kong, D. (2021). RNA polymerase III is required for the repair of DNA double-strand breaks by homologous recombination. Cell *184*, 1314–1329. https://doi.org/10.1016/j.cell.2021.01.048.

52. Šviković, S., Crisp, A., Tan-Wong, S.M., Guilliam, T.A., Doherty, A.J., Proudfoot, N.J., Guilbaud, G., and Sale, J.E. (2019). R-loop formation during S phase is restricted by PrimPol-mediated repriming. EMBO J. *38*, e99793. https://doi.org/10.15252/embj.201899793.

53. Nava, G.M., Grasso, L., Sertic, S., Pellicioli, A., Falconi, M.M., and Lazzaro, F. (2020). One, no one, and one hundred thousand: The many forms of ribonucleotides in DNA. Int. J. Mol. Sci. *21*, 1706. https://doi.org/10.3390/ijms21051706.

54. Crow, Y.J., Leitch, A., Hayward, B.E., Garner, A., Parmar, R., Griffith, E., Ali, M., Semple, C., Aicardi, J., Babul-Hirji, R., et al. (2006). Mutations in genes encoding ribonuclease H2 subunits cause Aicardi-Goutières syndrome and mimic congenital viral brain infection. Nat. Genet. *38*, 910–916. https://doi.org/10.1038/ng1842.

55. Rohman, M.S., Koga, Y., Takano, K., Chon, H., Crouch, R.J., and Kanaya, S. (2008). Effect of the disease-causing mutations identified in human ribonuclease (RNase) H2 on the activities and stabilities of yeast RNase H2 and archaeal RNase HII. FEBS J. *275*, 4836–4849. https://doi.org/10.1111/j.1742-4658.2008.06622.x.

56. Chon, H., Sparks, J.L., Rychlik, M., Nowotny, M., Burgers, P.M., Crouch, R.J., and Cerritelli, S.M. (2013). RNase H2 roles in genome integrity revealed by unlinking its activities. Nucleic Acids Res. *41*, 3130–3143. https://doi.org/10.1093/nar/gkt027.

57. Cerritelli, S.M., and El Hage, A. (2020). RNases H1 and H2: guardians of the stability of the nuclear genome when supply of dNTPs is limiting for DNA synthesis. Curr. Genet. *66*, 1073–1084. https://doi.org/10.1007/s00294-020-01086-8.

58. Meroni, A., Nava, G.M., Bianco, E., Grasso, L., Galati, E., Bosio, M.C., Delmastro, D., Muzi-Falconi, M., and Lazzaro, F. (2019). RNase H activities counteract a toxic effect of Polymerase in cells replicating with depleted dNTP pools. Nucleic Acids Res. *47*, 4612–4623. https://doi.org/10.1093/nar/gkz165.

59. Lemaçon, D., Jackson, J., Quinet, A., Brickner, J.R., Li, S., Yazinski, S., You, Z., Ira, G., Zou, L., Mosammaparast, N., et al. (2017). MRE11 and EXO1 nucleases degrade reversed forks and elicit MUS81-dependent fork rescue in BRCA2-deficient cells. Nat. Commun. *8*, 860. https://doi.org/10.1038/s41467-017-01180-5.

60. Dhoonmoon, A., Nicolae, C.M., and Moldovan, G.L. (2022). The KU-PARP14 axis differentially regulates DNA resection at stalled replication forks by MRE11 and EXO1. Nat. Commun. *13*, 5063. https://doi.org/10.1038/s41467-022-32756-5.

61. Jones, C.E., and Forsburg, S.L. (2021). Monitoring Schizosaccharomyces pombe genome stress by visualizing end-binding protein Ku. Biol. Open *10*, bio054346. https://doi.org/10.1242/bio.054346.

62. Mijic, S., Zellweger, R., Chappidi, N., Berti, M., Jacobs, K., Mutreja, K., Ursich, S., Ray Chaudhuri, A.,

Nussenzweig, A., Janscak, P., et al. (2017). Replication fork reversal triggers fork degradation in BRCA2-defective cells. Nat. Commun. *8*, 859. https://doi.org/10.1038/s41467-017-01164-5.

63. Neelsen, K.J., and Lopes, M. (2015). Replication fork reversal in eukaryotes: From dead end to dynamic response. Nat. Rev. Mol. Cell Biol. *16*, 207–220. https://doi.org/10.1038/nrm3935.

64. Maric, C., and Bénard, M. (2014). Replication forks reverse at high frequency upon replication stress in Physarum polycephalum. Chromosoma *123*, 577–585. https://doi.org/10.1007/s00412-014-0471-z.

65. Vengrova, S., and Dalgaard, J.Z. (2004). RNase-sensitive DNA modification(s) initiates S. pombe mating-type switching. Genes Dev. *18*, 794–804. https://doi.org/10.1101/gad.289404.

66. Hanada, K., Budzowska, M., Davies, S.L., Van Drunen, E., Onizawa, H., Beverloo, H.B., Maas, A., Essers, J., Hickson, I.D., and Kanaar, R. (2007). The structure-specific endonuclease Mus81 contributes to replication restart by generating double-strand DNA breaks. Nat. Struct. Mol. Biol. *14*, 1096–1104. https://doi.org/10.1038/nsmb1313.

67. Froget, B., Blaisonneau, J., Lambert, S., and Baldacci, G. (2008). Cleavage of stalled forks by fission yeast Mus81/Eme1 in absence of DNA replication checkpoint. Mol. Biol. Cell *19*, 445–456. https://doi.org/10.1091/mbc.E07-07-0728.

68. Sogo, J.M., Lopes, M., and Foiani, M. (2002). Fork reversal and ssDNA accumulation at stalled replication forks owing to checkpoint defects. Science (80-.). *297*, 599–602. https://doi.org/10.1126/science.1074023.

69. Hu, J., Sun, L., Shen, F., Chen, Y., Hua, Y., Liu, Y., Zhang, M., Hu, Y., Wang, Q., Xu, W., et al. (2012). The intra-S phase checkpoint targets Dna2 to prevent stalled replication forks from reversing. Cell *149*, 1221–1232. https://doi.org/10.1016/j.cell.2012.04.030.

70. Menin, L., Ursich, S., Trovesi, C., Zellweger, R., Lopes, M., Longhese, M.P., and Clerici, M. (2018). Tel1/ ATM prevents degradation of replication forks that reverse after topoisomerase poisoning. EMBO Rep. *19*, e45535. https://doi.org/10.15252/embr.201745535.

71. Griffiths, D.J.F., Liu, V.F., Nurse, P., and Wang, T.S.F. (2001). Role of fission yeast primase catalytic subunit in the replication checkpoint. Mol. Biol. Cell *12*, 115–128. https://doi.org/10.1091/mbc.12.1.115.

72. San Martin-Alonso, M., Soler-Oliva, M.E., García-Rubio, M., García-Muse, T., and Aguilera, A. (2021). Harmful R-loops are prevented via different cell cycle-specific mechanisms. Nat. Commun. *12*, 4451. https://doi.org/10.1038/s41467-021-24737-x.

73. Nemoz, C., Ropars, V., Frit, P., Gontier, A., Drevet, P., Yu, J., Guerois, R., Pitois, A., Comte, A., Delteil, C., et al. (2018). XLF and APLF bind Ku80 at two remote sites to ensure DNA repair by non-homologous end joining. Nat. Struct. Mol. Biol. *25*, 971–980. https://doi.org/10.1038/s41594-018-0133-6.

74. Dibitetto, D., Marshall, S., Sanchi, A., Liptay, M., Badar, J., Lopes, M., Rottenberg, S., and Smolka, M.B. (2022). DNA-PKcs promotes fork reversal and chemoresistance. Mol. Cell *82*, 3932-3942.e6. https://doi.org/10.1016/j.molcel.2022.08.028.

75. Reginato, G., and Cejka, P. (2020). The MRE11 complex: A versatile toolkit for the repair of broken DNA. DNA Repair (Amst). *91*–*92*, 102869. https://doi.org/10.1016/j.dnarep.2020.102869.

76. Langerak, P., Mejia-Ramirez, E., Limbo, O., and Russell, P. (2011). Release of Ku and MRN from DNA ends by Mre11 nuclease activity and Ctp1 is required for homologous recombination repair of double-strand breaks. PLoS Genet. *7*, e1002271. https://doi.org/10.1371/journal.pgen.1002271.

77. Reginato, G., Cannavo, E., and Cejka, P. (2017). Physiological protein blocks direct the Mre11-Rad50-Xrs2 and Sae2 nuclease complex to initiate DNA end resection. Genes Dev. *31*, 2325–2330. https://doi.org/10.1101/gad.308254.117.

78. Delamarre, A., Barthe, A., de la Roche Saint-André, C., Luciano, P., Forey, R., Padioleau, I., Skrzypczak, M., Ginalski, K., Géli, V., Pasero, P., et al. (2020). MRX Increases Chromatin Accessibility

at Stalled Replication Forks to Promote Nascent DNA Resection and Cohesin Loading. Mol. Cell *77*, 395-410.e3. https://doi.org/10.1016/j.molcel.2019.10.029.

79. Chang, E.Y.C., Tsai, S., Aristizabal, M.J., Wells, J.P., Coulombe, Y., Busatto, F.F., Chan, Y.A., Kumar, A., Dan Zhu, Y., Wang, A.Y.H., et al. (2019). MRE11-RAD50-NBS1 promotes Fanconi Anemia R-loop suppression at transcription–replication conflicts. Nat. Commun. *10*, 4265. https://doi.org/10.1038/s41467-019-12271-w.

80. Wang, W., Daley, J.M., Kwon, Y., Xue, X., Krasner, D.S., Miller, A.S., Nguyen, K.A., Williamson, E.A., Shim, E.Y., Lee, S.E., et al. (2018). A DNA nick at Ku-blocked double-strand break ends serves as an entry site for exonuclease 1 (Exo1) or Sgs1–Dna2 in long-range DNA end resection. J. Biol. Chem. *293*, 17061–17069. https://doi.org/10.1074/jbc.RA118.004769.

81. Daley, J.M., Tomimatsu, N., Hooks, G., Wang, W., Miller, A.S., Xue, X., Nguyen, K.A., Kaur, H., Williamson, E., Mukherjee, B., et al. (2020). Specificity of end resection pathways for double-strand break regions containing ribonucleotides and base lesions. Nat. Commun. *11*, 3088. https://doi.org/10.1038/s41467-020-16903-4.

82. Coquel, F., Silva, M.J., Técher, H., Zadorozhny, K., Sharma, S., Nieminuszczy, J., Mettling, C., Dardillac, E., Barthe, A., Schmitz, A.L., et al. (2018). SAMHD1 acts at stalled replication forks to prevent interferon induction. Nature *557*, 57–61. https://doi.org/10.1038/s41586-018-0050-1.

83. Pizzi, S., Sertic, S., Orcesi, S., Cereda, C., Bianchi, M., Jackson, A.P., Lazzaro, F., Plevani, P., and Muzi-Falconi, M. (2015). Reduction of hRNase H2 activity in Aicardi-Goutières syndrome cells leads to replication stress and genome instability. Hum. Mol. Genet. *24*, 649–658. https://doi.org/10.1093/hmg/ddu485.

84. Kramarz, K., Saada, A.A., and Lambert, S.A.E. (2021). The Analysis of Recombination-Dependent Processing of Blocked Replication Forks by Bidimensional Gel Electrophoresis. In Methods in Molecular Biology (Humana Press Inc.), pp. 365–381. https://doi.org/10.1007/978-1-0716-0644-5_25.

85. Sabatinos, S.A., and Forsburg, S.L. (2009). Measuring DNA content by flow cytometry in fission yeast. Methods Mol. Biol. *521*, 449–461. https://doi.org/10.1007/978-1-60327-815-7_25.

86. Knutsen, J.H.J., da Rein, I., Rothe, C., Stokke, T., Grallert, B., and Boye, E. (2011). Cell-cycle analysis of fission yeast cells by flow cytometry. PLoS One *6*, e17175. https://doi.org/10.1371/journal.pone.0017175.

Figure S1: Transient RNA:DNA hybrids accumulate at the *RTS1*-RFB (related to figure 1)

(A) Scheme of the *LacO*-marked RFB. mCherry-LacI (red ellipses) bound to *LacO* arrays (red), integrated ~7kb away from *ura4+*.

(B) Example of time-lapse microscopy to track Rnh1-D129N-GFP (green signal) recruitment to the *LacO*-marked RFB (Red dot) in RFB ON condition. Time is indicated in seconds. Septated cells are considered in S-phase. White arrow indicates colocalization between Rnh1 and *LacO*-marked RFB.

(C) Quantification of co-localization events in indicated conditions. Septated cells were considered in S-phase and mono-nucleated cells were considered in G2. Dots represent values obtained from independent biological replicates. Bars indicate mean values ± standard deviation (SD). Statistical analysis was performed using student's t-test, compared to RFB OFF condition.

(D) Diagram depicting the duration of co-localization events measured in S-phase in RFB ON condition.
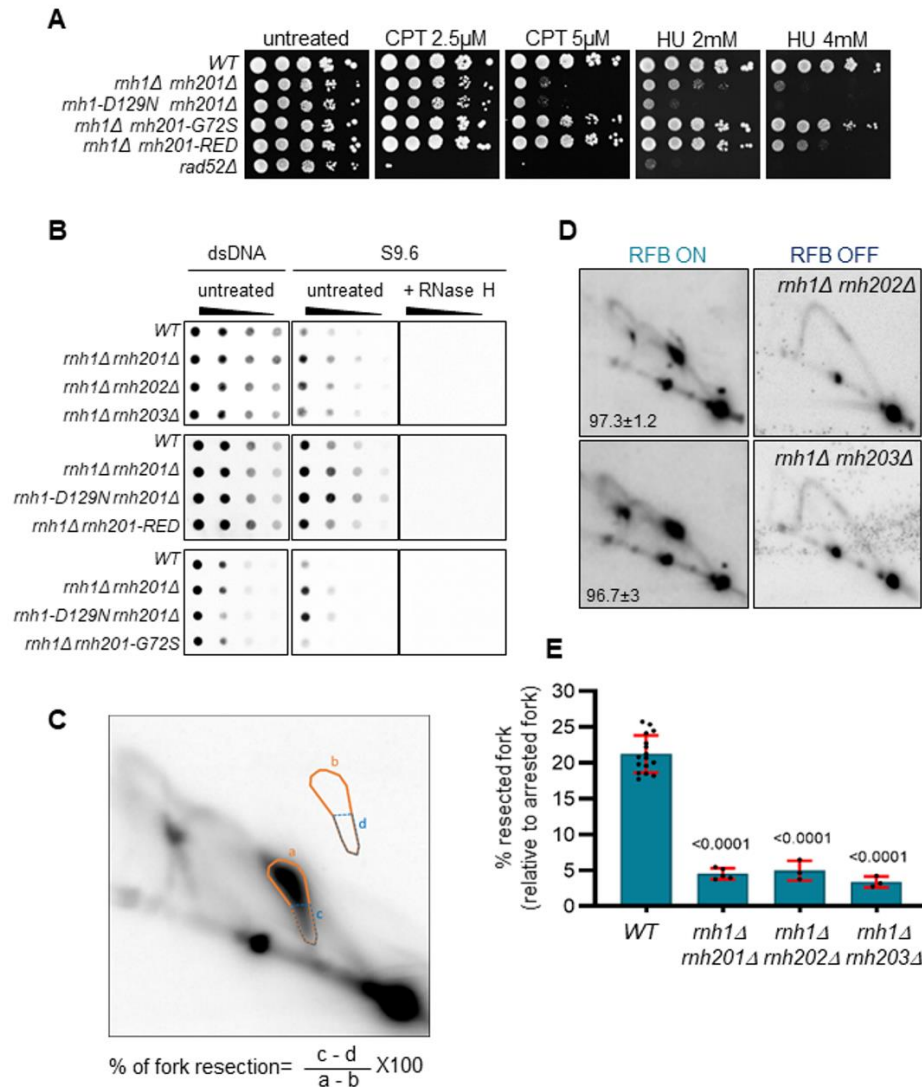
Figure S2: The lack of RNase H activities leads to a defect in nascent strand degradation (related to figure 1 and 2).

(A) Tenfold serial dilutions of indicated strains on indicated media conditions (CPT: camptothecin, HU: hydroxyurea).

(B) RNA:DNA hybrid accumulation was analyzed by dot blot in indicated strains. Nucleic acid extracts were treated with RNase H, or not. Membranes were probed with the S9.6 or dsDNA antibodies.

(C) Schematic of the "tail" quantification procedure from 2DGE blots.

(D) Representative 2DGE analysis in indicated strains and conditions. Numbers indicate the efficiency of the RFB ± SD.

(E) "Tail" quantification. Dots represent values obtained from independent biological replicate. Bars indicate mean values ± SD. Statistical analysis was performed using student's t-test, compared to *WT*.

A

RFB ON

WT — 96.9
rnh201Δ — 97.5
rad50Δ — 97±0.9
rad50Δ rnh201Δ — 97.2±0.2

B

% resected fork (relative to arrested fork)

WT, rnh201Δ, rad50Δ, rnh201Δ rad50Δ, rad50Δ*

ns

C

Frequency of RFB-induced RS (X 10⁻³)

WT, rnh201Δ, rad50Δ, rnh201Δ rad50Δ

0.0001
0.0001
0.0001
ns

D

WT, rnh201Δ, ctp1Δ, pku70Δ, rnh201Δ ctp1Δ, ctp1Δ pku70Δ, rnh201Δ ctp1Δ pku70Δ, rad52Δ

untreated | CPT 0.25µM | CPT 0.5µM | HU 2mM | HU 3mM | MMS 0.001% | MMS 0.002%

E

WT, rnh201Δ, rad50Δ, mre11-D65N, rnh201Δ rad50Δ, rnh201Δ mre11-D65N, rad52Δ

untreated | CPT 0.125µM | CPT 0.25µM | CPT 0.5µM

WT, rnh201Δ, rad50Δ, mre11-D65N, rnh201Δ rad50Δ, rnh201Δ mre11-D65N, rad52Δ

HU 1mM | HU 2mM | HU 3mM

F

RFB ON | RFB OFF

mre11-D65N — 98.7±0.4
rnh201Δ mre11-D65N — 98.5±0.1

G

% resected fork (relative to arrested fork)
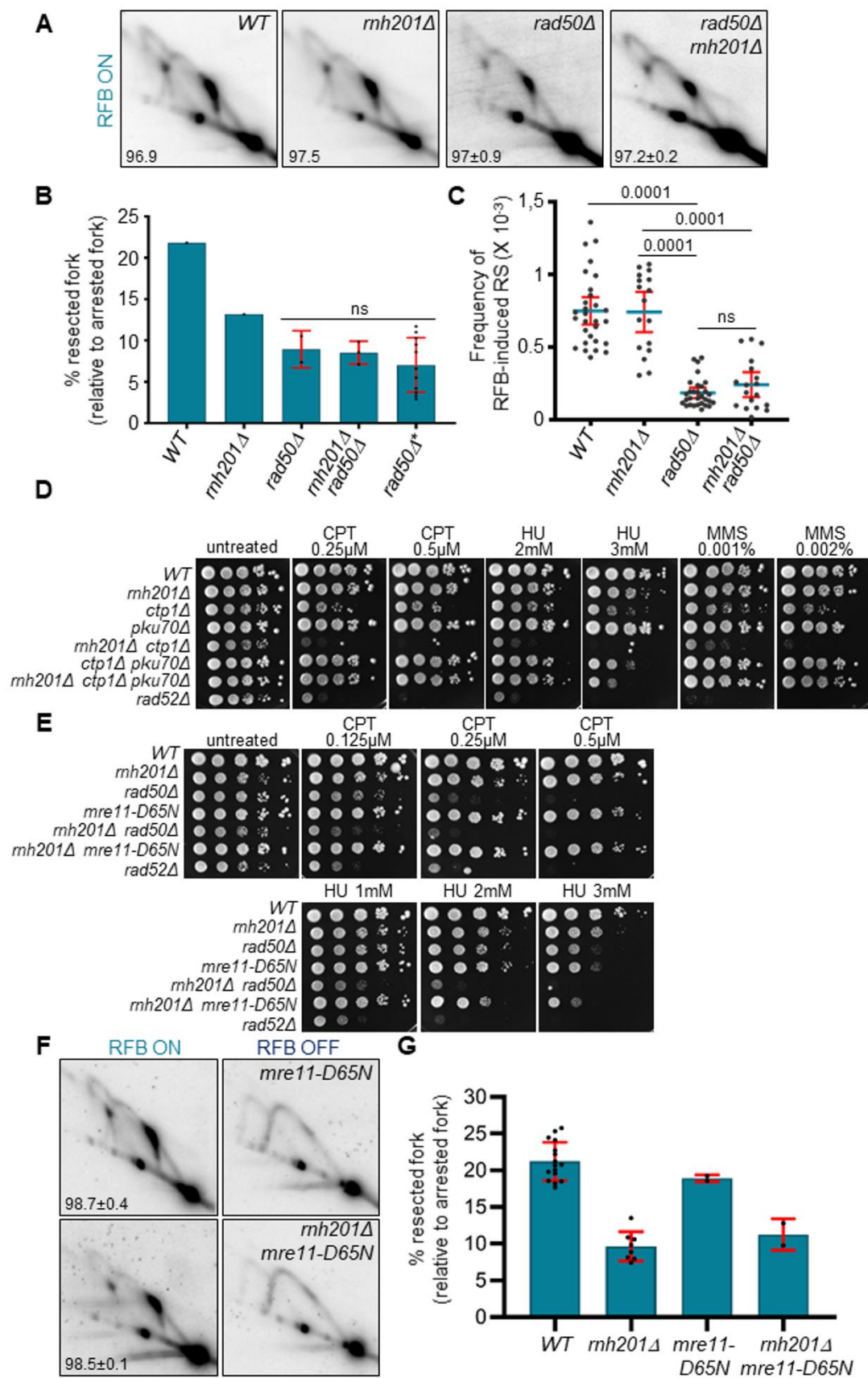
WT, rnh201Δ, mre11-D65N, rnh201Δ mre11-D65N

41

Figure S3: RNase H2 co-operates with MRN to promote cell resistance to replication stress (related to Figure 3).

(A) Representative 2DGE analysis in indicated strains and in RFB ON condition. Numbers indicate the efficiency of the RFB ± SD.

(B) "Tail" quantification. Dots represent values obtained from independent biological replicate. Bars indicate mean values ± SD. Statistical analysis was performed using student's t-test. Values for *rad50Δ** correspond to the ones obtained in Teixeira-Silva 2017.

(C) Frequency of RFB-induced RS in indicated strains and conditions. Each dot represents one sample from independent biological replicate. Bars indicate mean values ± 95 % confidence interval. Statistics were calculated using Mann-Whitney U test.

(D) And (E) Tenfold serial dilution of indicated strains on indicated media conditions (CPT: camptothecin, HU: hydroxyurea, MMS: methyl methane sulfonate).

(F) Representative 2DGE analysis in indicated strains and conditions. Numbers indicate the efficiency of the RFB ± SD.

(G) "Tail" quantification. Dots represent values obtained from independent biological replicate. Bars indicate mean values ± SD.
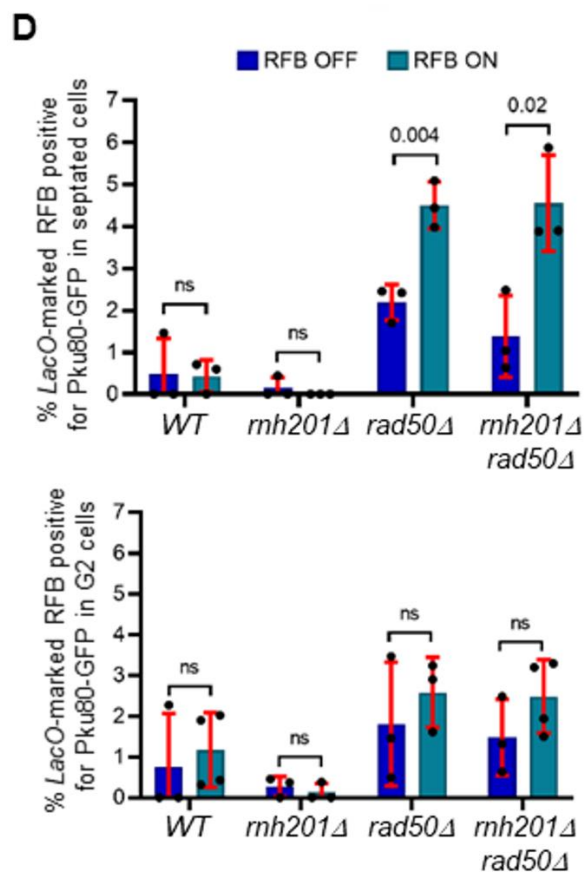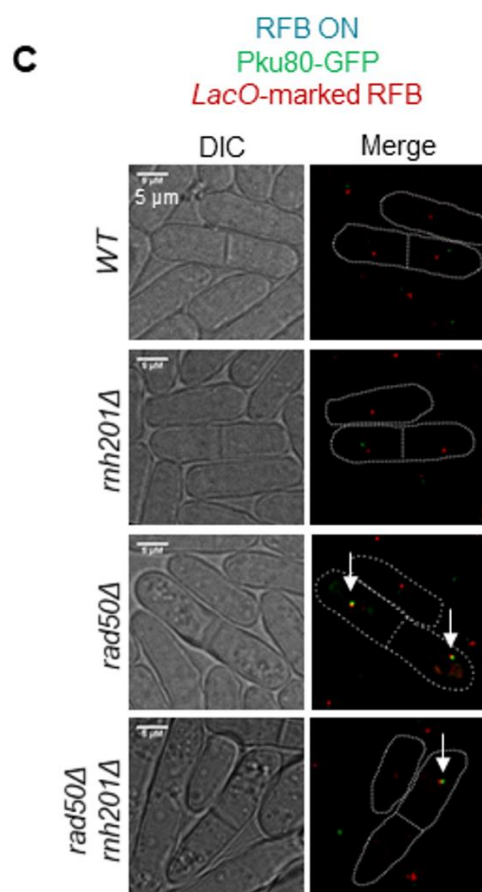
A

Untreated | + CPT

WT, rnh201Δ, rad50Δ, rad50Δ rnh201Δ

DIC Pku80-GFP DIC Pku80-GFP

5 µm

B

☐ untreated ■ CPT 20µM 4h

<0.014

ns

ns

% of cells showing Pku80-GFP

WT   rnh201Δ   rad50Δ   rnh201Δ rad50Δ

C

RFB ON
Pku80-GFP
LacO-marked RFB

DIC Merge

WT, rnh201Δ, rad50Δ, rad50Δ rnh201Δ

5 µm

D

■ RFB OFF ■ RFB ON

% *LacO*-marked RFB positive for Pku80-GFP in septated cells

0.004   0.02

ns   ns

WT   rnh201Δ   rad50Δ   rnh201Δ rad50Δ

% *LacO*-marked RFB positive for Pku80-GFP in G2 cells

ns   ns   ns   ns

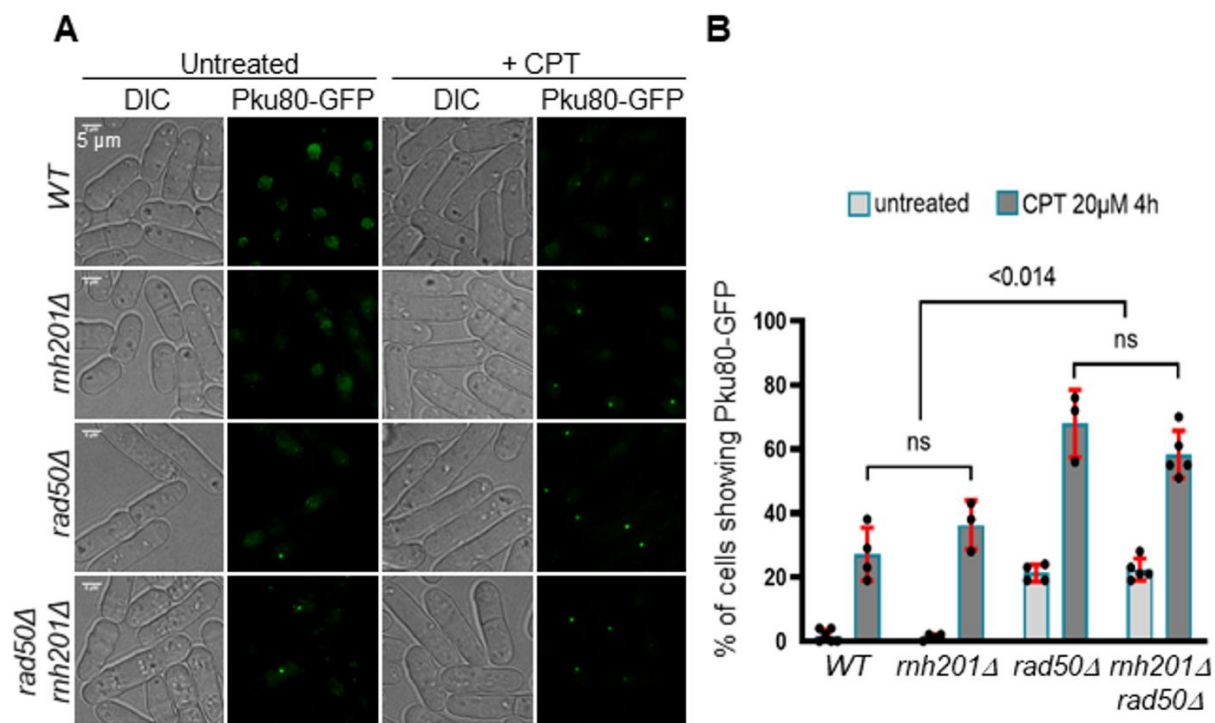WT   rnh201Δ   rad50Δ   rnh201Δ rad50Δ

43

Figure S4: Ku accumulation upon replication-born DNA damage is RNase H2 independent (related to Figure 3).

(A) Examples of cells showing Pku80-GFP foci in indicated strains and conditions (CPT at 20µM for 4 hours).

(B) Quantification of panel A. Dots represent values obtained from independent biological replicates. Bars indicate mean values ± SD. For each experiment, 200 to 300 nuclei were analyzed. Statistical analysis was performed using student's t-test.

(C) Examples of Pku80-GFP (green foci) co-localizing with the *LacO*-marked RFB (visualized by LacI-mCherry dot). White arrows indicate co-localization events.

(D) Quantification of panel C. Dots represent values obtained from independent biological replicate. Bars indicate mean values ± SD. For each experiment, 100 to 200 nuclei were analyzed. The high background of co-localization events *in rad50Δ* cells in RFB OFF condition are likely caused by the leaky expression of the Rtf1 protein that binds to the *RTS1* sequence. Statistical analysis was performed using student's t-test.
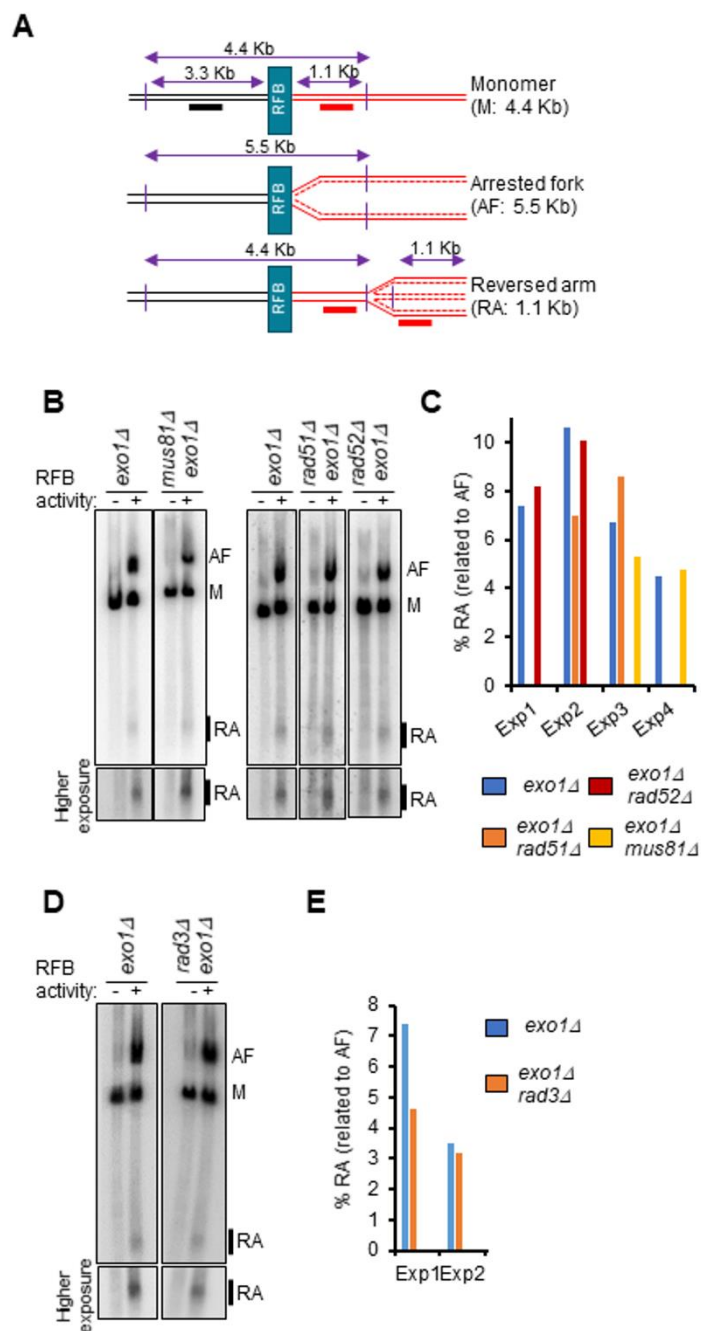
Figure S5: HR, Rad3 and Mus81-independent accumulation of the reversed linear fragment at the RFB (related to Figure 4)

(A) Scheme of the construct used with the expected mass of RI species and the probes used (Probe 1 and 2 in black and red, respectively).

(B) and (D) Representative Southern-blot analysis after 1DGE resolution of RIs in indicated strains and conditions, using the red probe. A higher exposure of the RA is shown.

(C) and (E) RA quantification (relative to AF signal) in indicated strains and experiments.
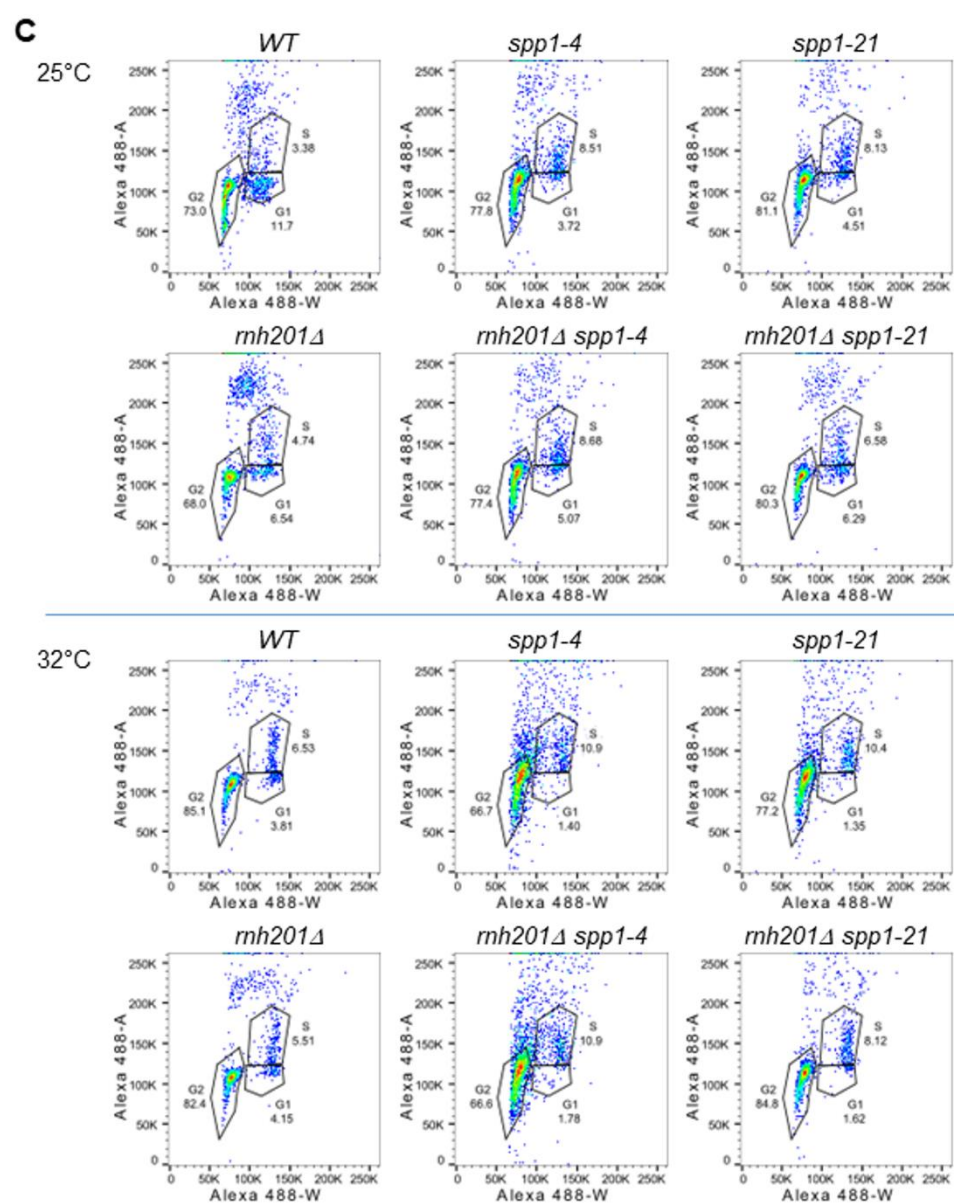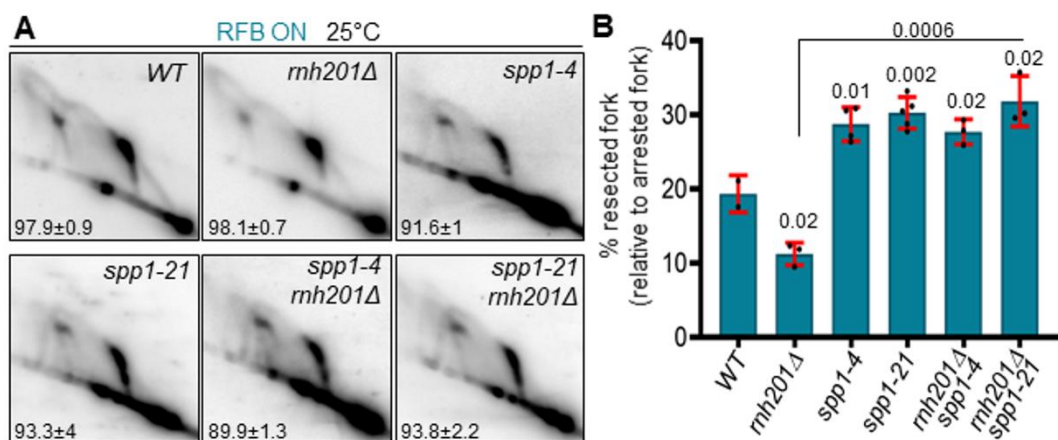
Figure S6: The requirement of RNaseH2 in nascent strand degradation requires the catalytic subunit of the primase (related to Figure 5).

(A) Representative 2DGE analysis in indicated strains and in RFB ON conditions. Numbers indicate the efficiency of the RFB ± SD. Strains were grown at 25°C.

(B) "Tail" quantification. Dots represent values obtained from independent biological replicate. Bars indicate mean values ± SD. Statistical analysis was performed using student's t-test.

(C) Cell Cycle analysis of indicated strains grown at 25°C (top panels) or grown at 25°C then switched at 32°C for 19 hours (bottom panels). The % of cells in G2, G1 and S-phase are indicated on each scatter plot.
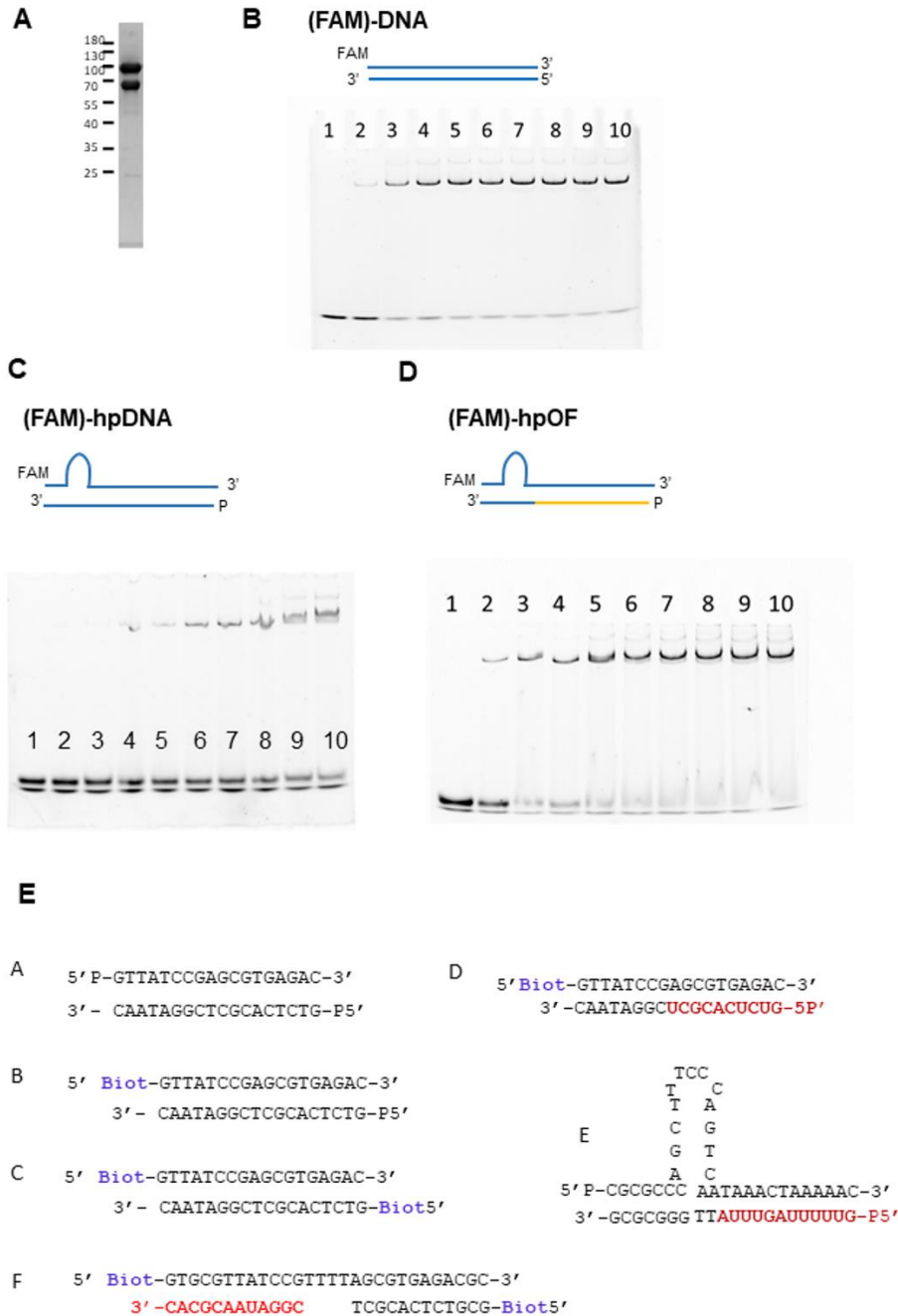
Figure S7: Calorimetry and EMSA of SpKu (related to Figure 6)

(A) Purified *S. pombe* Ku70-80 heterodimer.

(B-D) EMSA of SpKu versus dsDNA labeled with FAM (B), SpKu versus dsDNA containing an hairpin labeled with FAM (C), and SpKu versus dsDNA containing an hairpin and an OF at one extremity (D). Columns: 1(no SpKu), 2 (10nM SpKu), 3 (25nM SpKu), 4 (50nM SpKu), 5 (75nM SpKu), 6 (100nM SpKu), 7 (150nM SpKu), 8 (200nM SpKu), 9 (250nM SpKu) and 10 (400nM SpKu).

(E) Sequences of oligonucleotides A to F used in Figure 6.

Supplementary Table 1: Strains used in this study (related to the Key resources table of the STAR method section).

Strain number	Mating type	Genotype	Reference
SL3494	*h-*	*nmt41:rtf1:sup35 t-ura4-sd20<ori ade6-704 leu1-32*	This study
SL3319	*h+*	*rnh1::hygro nmt41:rtf1:sup35 t-ura4-sd20<ori ade6-704 leu1-32*	This study
SL3496	*h+*	*rnh201::kan nmt41:rtf1:sup35 t-ura4-sd20<ori ade6-704 leu1-32*	This study
SL2346	*h+*	*rnh202::hygro nmt41:rtf1:sup35 t-ura4-sd20<ori ade6-704 leu1-32*	This study
SL2365	*h-*	*rnh203::hygro nmt41 :rtf1 :sup35 t-ura4-sd20<ori ade6-704 leu1-32*	This study
SL3197	*h-*	*rnh1::hygro rnh201::kan nmt41:rtf1:sup35 t-ura4-sd20<ori ade6-704 leu1-32*	This study
SL2453	*h-*	*rnh1::hygro rnh202::hygro nmt41:rtf1:sup35 t-ura4-d20<ori ade6-704 leu1-32*	This study
SL2677	*h-*	*rnh1::hygro rnh203::hygro nmt41:rtf1:sup35 t-ura4-d20<ori ade6-704 leu1-32*	This study
SL0680	*h-smt0*	*rad52::kan nmt41:rtf1:sup35 t-ura4+<ori ade6-704 leu1-32*	Lambert et al., 2010
SL3312	*h+*	*ssb3-YFP:nat nmt41:rtf1:sup35 t-ura4-sd20<ori ade6-704 leu1-32*	This study
SL2038	*h+*	*rnh1::hygro rnh201::kan ssb3-YFP:nat nmt41:rtf1:sup35 t-ura4-sd20<ori ade6-704 leu1-32*	This study
SL1672	*h+*	*rnh1-D129N-GFP:kan arg3::psv40-mcherry-LacI** ade6-704 leu1-32 nmt41:rtf1:sup35 LacO 7.9Kb:kan t-ura4+<ori*	This study
SL1999	*h-*	*rnh1-D129N-GFP:kan nmt41:rtf1:sup35 t-ura4-sd20<ori ade6-704 leu1-32*	This study
SL3518	*h+*	*rnh201-G72S nmt41:rtf1:sup35 t-ura4-sd20<ori ade6-704 leu1-32*	This study
SL3262	*h-*	*loxP-rnh201RED(P75D-Y245A)-kanMX6-loxM3 nmt41:rtf1:sup35 t-ura4-sd20<ori ade6-704 leu1-32*	This study
SL3510	*h+*	*rad3::hygro nmt41:rtf1:sup35 t-ura4-sd20<ori ade6-704 leu1-32*	This study
SL3514	*h-*	*rad3::hygro rnh201::kan nmt41:rtf1:sup35 t-ura4-sd20<ori ade6-704 leu1-32*	This study
SL2032	*h+*	*rnh1::hygro ssb3-YFP:nat nmt41:rtf1:sup35 t-ura4-sd20<ori ade6-704 leu1-32*	This study
SL2035	*h+*	*rnh201::kan ssb3-YFP:nat nmt41:rtf1:sup35 t-ura4-sd20<ori ade6-704 leu1-32*	This study
SL1990	*h-*	*rnh1-D129N-GFP:kan rnh201::kan nmt41:rtf1:sup35 t-ura4-sd20<ori ade6-704 leu1-32*	This study
SL3343	*h-*	*rnh1::hygro rnh201-G72S nmt41:rtf1:sup35 t-ura4-sd20<ori ade6-704 leu1-32*	This study

SL3272	*h-*	*rnh1::hygro loxP-rnh201RED(P75D-Y245A)-kanMX6-loxM3 nmt41:rtf1:sup35 t-ura4-sd20<ori ade6-704 leu1-32*	This study
SL2407	*h-*	*rad50::kan nmt41:rtf1:sup35 t-ura4-sd20<ori ade6-704 leu1-32*	This study
SL3498	*h+*	*pku70::hygro nmt41:rtf1:sup35 t-ura4-sd20<ori ade6-704 leu1-32*	This study
SL3257	*h-*	*rnh201::kan rad50::kan nmt41:rtf1:sup35 t-ura4-sd20<ori ade6-704 leu1-32*	This study
SL2409	*h-*	*rad50::kan pku70::hygro nmt41:rtf1:sup35 t-ura4+<ori ade6-704 leu1-32*	This study
SL2415	*h+*	*rnh201::kan rad50::kan pku70::hygro nmt41:rtf1:sup35 t-ura4-sd20<ori ade6-704 leu1-32*	This study
SL3264	*h+*	*rad50::kan loxP-rnh201RED(P75D-Y245A)-kanMX6-loxM3 nmt41:rtf1:sup35 t-ura4-sd20<ori ade6-704 leu1-32*	This study
SL3583	*h+*	*rad50::kan rnh201-G72S nmt41:rtf1:sup35 t-ura4-sd20<ori ade6-704 leu1-32*	This study
SL3502	*h-*	*rnh201::kan pku70::hygro nmt41:rtf1:sup35 t-ura4-sd20<ori ade6-704 leu1-32*	This study
SL3508	*h+*	*rnh201::kan pku70::hygro exo1::nat nmt41:rtf1:sup35 t-ura4-sd20<ori ade6-704 leu1-32*	This study
SL3501	*h-*	*exo1::nat nmt41:rtf1:sup35 t-ura4-sd20<ori ade6-704 leu1-32*	This study
SL2009	*h+*	*pku70::leu2 rnh1::hygro rnh201::kan nmt41:rtf1:sup35 t-ura4-sd20<ori ade6-704 leu1-32*	This study
SL2431	*h+*	*ctp1::hygro nmt41:rtf1:sup35 t-ura4-sd20<ori ade6-704 leu1-32*	This study
SL2285	*h+*	*ctp1::hygro rnh201::kan nmt41:rtf1:sup35 t-ura4-sd20<ori ade6-704 leu1-32*	This study
SL2617	*h-*	*ctp1::hygro pku70::hygro nmt41:rtf1:sup35 t-ura4-sd20<ori ade6-704 leu1-32*	This study
SL2433	*h+*	*ctp1::hygro rnh201::kan pku70::hygro nmt41:rtf1:sup35 t-ura4-sd20<ori ade6-704 leu1-32*	This study
SL3687	*h+*	*mre11-D65N nmt41:rtf1:sup35 t-ura4-sd20<ori ade6-704 leu1-32*	This study
SL3689	*h+*	*rnh201::kan mre11-D65N nmt41:rtf1:sup35 t-ura4-sd20<ori ade6-704 leu1-32*	This study
SL3526	*h+*	*pku80-GFP:kan arg3::psv40-mcherry-LacI** ade6-704 leu1-32 nmt41:rtf1:sup35 LacO 7.9Kb:kan t-ura4+<ori*	This study
SL3531	*h+*	*rnh201::kan pku80-GFP:kan arg3::psv40-mcherry-LacI** ade6-704 leu1-32 nmt41:rtf1:sup35 LacO 7.9Kb:kan t-ura4+<ori*	This study
SL3534	*h+*	*rad50::kan pku80-GFP:kan arg3::psv40-mcherry-LacI** ade6-704 leu1-32 nmt41:rtf1:sup35 LacO 7.9Kb:kan t-ura4+<ori*	This study
SL3538	*h-*	*rnh201::kan rad50::kan pku80-GFP:kan arg3::psv40-mcherry-LacI** ade6-704 leu1-32 nmt41:rtf1:sup35 LacO 7.9Kb:kan t-ura4+<ori*	This study

SL0504	h-	nmt41:rtf1:sup35 t<ura4+-ori ade6-704 leu1-32	This study
II535	h-	rad50::kan exo1::nat nmt41:rtf1:sup35 t-ura4-sd20<ori ade6-704 leu1-32	This study
II539	h-	rad50::kan exo1::nat nmt41:rtf1:sup35 t<ura4-sd20-ori ade6-704 leu1-32	This study
II272	h+	exo1::nat nmt41:rtf1:sup35 ade6-704 leu1-32 [AscI-ura4+-RTS1]	This study
II209	h-	nmt41:rtf1:sup35 ade6-704 leu1-32 [AscI-ura4+-RTS1]	This study
SL2460	h+	cdc25 exo1::nat nmt41:sup35:rtf1 ade 6-704 leu1-32 [AscI-RTS1-ura4+]	This study
SL2445	h-	rnh201::kan exo1::nat nmt41:rtf1:sup35 ade6-704 leu1-32 [AscI-ura4+-RTS1]	This study
SL2533	h+	rnh1::hygro rnh201::kan exo1::nat nmt41:rtf1:sup35 ade6-704 leu1-32 [AscI-ura4+-RTS1]	This study
SL2264	h+	rad52::kan exo1::nat rtf1:nmt41:sup35 ade6-704 leu1-32 [AscI-ura4+-RTS1]	This study
SL2240	h-smt0	rad51::kan exo1::nat rtf1:nmt41:sup35 ade6-704 leu1-32 [AscI-ura4+-RTS1]	This study
SL2249	h-	mus81::kan exo1::nat rtf1:nmt41:sup35 ade6-704 leu1-32 [AscI-ura4+-RTS1]	This study
SL3834	h+	spp1-4:ura4+ nmt41:rtf1:sup35 t-ura4-sd20<ori ade6-704 leu1-32	This study
SL3840	h-	spp1-4:ura4+ rnh201::kan nmt41:rtf1:sup35 t-ura4-sd20<ori ade6-704 leu1-32	This study
SL3836	h-	spp1-21:ura4+ nmt41:rtf1:sup35 t-ura4-sd20<ori ade6-704 leu1-32	This study
SL3839	h-	spp1-21:ura4+ rnh201::kan nmt41:rtf1:sup35 t-ura4-sd20<ori ade6-704 leu1-32	This study
SL2062	h-	sen1::nat nmt41:rtf1:sup35 t-ura4-sd20<ori ade6-704 leu1-32	This study
SL3221	h-	rad2::kan nmt41:rtf1:sup35 t-ura4-sd20<ori ade6-704 leu1-32	This study
SL3347	h-	rad2::kan pku70::hygro nmt41:rtf1:sup35 t-ura4-sd20<ori ade6-704 leu1-32	This study
SL3862		spp1-4:ura+ pku80-GFP:kan arg3::psv40-mcherry-LacI** leu1-32 ade6-704 nmt41:rtf1:sup35 LacO 7.9Kb:kan t-ura4+<ori	This study
SL3863		spp1-21:ura+ pku80-GFP:kan arg3::psv40-mcherry-LacI** leu1-32 ade6-704 nmt41:rtf1:sup35 LacO 7.9Kb:kan t-ura4+<ori	This study

Supplementary Table 2: list of primers used in this study

Name	Distance (pb) from the *RTS1*-RFB position	Sequence (5'→3')
AseICen		GTCAAGTAAAACGTTGAATCG
Ura4-2F	-900	TGATATGAGCCCAAGAAGCA
Ura4-2R		CAAATTCGCAGACATTGGAA
L5F	-110	AGGGCATTAAGGCTTATTTACAGA
L5R		TCACGTTTAATTTCAAACATCCA
L3F	110	TTTAAATCAAATCTTCCATGCG
L3R		TGTACCCATGAGCAAACTGC
L400F	400	ATCTGACATGGCATTCCTCA
L400R		GATGCCAGACCGTAATGACA
L600F	600	CCATTGACTAGGAGGACTTTGAG
L600R		CCCTGGCGGTTGTAGTTAGT
L900F	900	AACGGTTGTAGAAGACGAGCA
L900R		TGTAAGCACACCTTCAATGTATCA
L1400F	1400	AACATCGGTGACCTCGTTCT
L1400R		CTCTTCGCTCCAAGCGTTAT
EMSA experiments		
FAM-DNA up		5'-(FAM)GTTATCCGAGCGTGAGAC-3'
FAM-DNA down		5'-GTCTCACGCTCGGATAAC-3'
FAM-hpDNA up		5'-(FAM)-CGCGCCCAGCTTTCCCAGCTAATAAACTAAAAAC-3'
FAM-hpDNA down		5'-(P)GTTTTTAGTTTATTGGGCGCG-3'.
FAM-hpOF up		5'-(FAM)-CGCGCCCAGCTTTCCCAGCTAATAAACTAAAAAC-3'
FAM-hpOF down		5'- (P) <u>GUUUUUAGUUUA</u> TTGGGCGCG-3'
A-up		5'-(P)GTTATCCGAGCGTGAGAC-3'
A and B-down		5'-(P) GTCTCACGCTCGGATAAC-3'
B, C and D-up		5'(Biot)-GTTATCCGAGCGTGAGAC-3'
C-down		5'-(Biot) GTCTCACGCTCGGATAAC-3'
D-down		5'-<u>GUCUCACGCU</u>CGGATAAC-3'
E-up		5'-CGCGCCCAGCTTTCCCAGCTAATAAACTAAAAAC-3'
E-down		5'- (P) <u>GUUUUUAGUUUA</u> TTGGGCGCG-3'
F-up		5'-(Biot)GTGCGTTATCCGTTTTAGCGTGAGACGC-3'
F-down part1		5'-(Biot)GCGTCTCACGCT-3'
F-down part2		5'-<u>CGGAUAACGCAC</u>-3'